

Soil geochemistry as a driver of soil organic matter composition: insights from a soil chronosequence

Moritz Mainka¹, Laura Summerauer², Daniel Wasner², Gina Garland^{2,3}, Marco Griepentrog², Asmeret Asefaw Berhe⁴, and Sebastian Doetterl²

5 ¹Institute of Landscape and Plant Ecology, Universität Hohenheim, Stuttgart, 70599, Germany

²Department of Environmental System Science, ETH Zürich, Zürich, 8092, Switzerland

³Agroscope, Soil Quality and Use group, 8046 Zurich, Switzerland

⁴Department of Earth Sciences, Life & Environmental Sciences, University of California, Merced, 95343, USA

Correspondence to: Sebastian Doetterl (sdoetterl@usys.ethz.ch)

10 **Abstract.** A central question in carbon research is how stabilization mechanisms in soil change over time with soil development and how this is reflected in qualitative changes of soil organic matter (SOM). To address this matter, we assessed the influence of soil geochemistry on bulk SOM composition along a soil chronosequence in California, USA spanning 3 million years. This was done by combining data on soil mineralogy and texture from previous studies with additional measurements on total carbon (C), stable isotope values ($\delta^{13}\text{C}$ and $\delta^{15}\text{N}$), and spectral information derived from Diffuse Reflectance Infrared Fourier-Transform Spectroscopy (DRIFTS). To assess qualitative shifts in bulk SOM, we analysed the peak areas of simple plant-derived (S-POM), complex plant-derived (C-POM), and predominantly microbially derived OM (MOM) and their changes in abundance across soils varying several millennia to millions of years in weathering and soil development. We observed that SOM became increasingly stabilized and microbially-derived (lower C:N ratio, increasing $\delta^{13}\text{C}$ and $\delta^{15}\text{N}$) as soil weathering progressed. Peak areas of S-POM (i.e. aliphatic root exudates) did not change over time, while peak areas of C-POM (lignin) and MOM (components of microbial cell walls (amides, quinones, and ketones)) increased over time and depth and were closely related to clay content and pedogenic iron oxides. Hence, our study suggests that with progressing soil development, SOM composition co-varies with changes in the mineral matrix. Our study indicates that a discrimination in favour of structurally more complex OM compounds (C-POM, MOM) gains play an increasingly gained important role in soil carbon stabilization mechanisms as the mineral soil matrix becomes increasingly weathered.

15
20
25 **Keywords:** SOM composition, DRIFTS, ^{13}C , ^{15}N , SOM stabilization, soil chronosequence, organo-mineral association.

1 Introduction

Soils harbour the largest and most active terrestrial carbon (C) pool on earth (Jobbágy and Jackson, 2000; Lal, 2008). Over the past decades, many of the detailed mechanistic processes determining the fate of soil organic matter (SOM) in soils have been well studied (Schmidt et al., 2011; Lehmann and Kleber, 2015; Kleber et al., 2021). Yet, it remains unclear how these individual processes evolve over time as stabilization mechanisms depend on the soil matrix properties which in turn is subject to constant

30

changes through soil formation (Bradford et al., 2016; Bailey et al., 2019; Kögel-Knabner and Amelung, 2021). ~~Additionally~~Further, differences regarding pedogenic (i.e. soil type, mineralogy, soil microbiome) and environmental (i.e. climate, vegetation cover) properties not only determine the sizes of SOM stocks, but also govern the abundance of diverse biochemical compounds (e.g. lignin, polysaccharides, lipids) found in the terrestrial C pool (Paul, 2016; Hall et al., 2020).

35 Hence, SOM composition (the prevalence of certain biochemical compounds) may serve as a proxy for ecosystem properties and soil functioning, as it ~~responds to land use change (Durrer et al., 2021) and~~ affects C cycling by the amount of energy provided to soil microorganisms (Nunan et al., 2015; Barré et al., 2016). Furthermore, the peak areas related to biochemical SOM compounds has been successfully used to parameterize fast and slow-cycling SOM pools (Todd-Brown et al., 2013; Bailey et al., 2018; Laub et al., 2020; Baldock et al., 2021).

40 Despite the central role that SOM composition plays in soil C cycling, we lack a thorough understanding of how it is influenced by the input of organic matter (OM), and by changes of soil C stabilization mechanisms following soil formation (von Lützow et al., 2008; Doetterl et al., 2018). At initial soil formation stages, the mainly plant-derived input material determines SOM composition (Khedim et al., 2021). With increasing soil age, soil properties such as soil mineralogy, ~~and~~ texture, and soil aggregation become increasingly important for the stabilization of accumulating SOM (Chorover et al., 2004; Mikutta et al.,

45 2006; Mikutta et al., 2009; Wei et al. 2016). For example, a comparative study of soil aggregation in relation to soil weathering found micro- and macroaggregates to become more stable with increasing weathering (Wei et al., 2016). In addition, ~~t~~There is an emerging consensus that certain SOM compounds are preferentially bound to mineral surfaces in organo-mineral associations (OMA) and are thus highly important C stabilization mechanisms (Kleber et al., 2021). Many studies reported high affinity of chemically simple carbohydrates to minerals (i.e. low molecular weight compounds from root

50 exudates or microbial origin) (Kaiser et al., 1997; Calderón et al., 2011; Kleber et al., 2011; Cotrufo et al., 2015; Lavalée et al., 2019). Conversely, chemically more complex compounds (i.e. lignin or phenols from woody plant parts), formerly considered to be recalcitrant OM, were found to be less associated with minerals (Spielvogel et al., 2008; Kleber et al., 2011; Lavalée et al., 2019). However, recent studies reported a preferential binding with iron oxides in the particular case of lignin (Kramer et al., 2012; Hall et al., 2016).

55 OMAs are preferentially found in the fine-grained, heavy soil fraction ($< 2 \mu\text{m}$ = clay) which is therefore often regarded as the most important fraction to explain how SOM persists in soils (Six et al., 2000; Kleber et al., 2021). Recent conceptualizations argue that the organo-mineral interaction is subject to dynamic changes through mineral weathering (Cotrufo et al., 2013; Lehmann and Kleber 2015; Kleber et al., 2021). With ongoing soil weathering, primary silicates originating from the parent material are replaced by newly formed secondary clay minerals (White et al., 1996). The sorptive capacity of clay minerals

60 ~~thereby~~ decreases as 2:1 layer type silicates (e.g. smectite) are substituted by 1:1 layer type silicates (e.g. kaolinite) (Sposito et al., 1999). In contrast, iron oxides, particularly nano-sized iron- (Fe) and aluminium-bearing (Al) oxides, gain importance with increasing soil weathering as they conserve high specific surface areas. ~~Moreover, oxides become positively charged~~

~~(protonated) at low pH values allowing for ligand exchange with OM compounds. As soil acidification progresses with soil weathering, the importance of these oxides to stabilize OM compounds becomes more pronounced~~ (Kleber et al., 2021). Hence,

65 the potential of different SOM stabilization mechanisms changes dynamically as a function of mineral weathering (Mikutta et al., 2009). Given that different SOM compounds have differing binding preferences, mineral weathering is thus likely to affect SOM composition. Therefore, a promising approach to gain further insights into the controls of SOM composition is the observation of changes in SOM composition along pedogenic gradients.

~~We sampled from an undisturbed soil chronosequence spanning 3 million years, located under rangeland vegetation in the Mediterranean climatic conditions of California, USA. We used diffuse reflectance infrared Fourier transform spectroscopy (DRIFTS) to characterize the SOM composition. DRIFTS is a spectroscopic technique commonly used for soil samples and provides spectroscopic information based on the absorbance after an infrared beam hits soil samples. This technique can be used to semi-quantitatively assess the peak areas of different SOM functional groups (Ellerbroek and Gerke 2004; Parikh et al., 2014; Margenot et al., 2015; Margenot et al., 2017). The spectral information derived from DRIFTS is supported by stable isotope signatures ($\delta^{13}\text{C}$ and $\delta^{15}\text{N}$ values) and the soil C:N ratio, both of which are strongly associated with SOM dynamics (Dijkstra et al., 2006; Conen et al., 2008; Brunn et al., 2016).~~

The aim of our study was to assess how bulk SOM composition changed along an undisturbed soil chronosequence spanning 3 million years, located under rangeland vegetation in the Mediterranean climatic conditions of California, USA, a gradient of soil mineralogy and texture associated with soil development. To this end, we used the C:N ratio and the stable isotope signatures $\delta^{15}\text{N}$ and $\delta^{13}\text{C}$ as proxies for the degree of microbial transformation of the bulk SOM, and the selected peak areas of DRIFTS measurements as proxies for SOM composition. We then combined this information with previously published data on soil mineralogy and texture from the same samples (Doetterl et al., 2018) in order to identify which drivers are most important in explaining shifts in SOM composition with soil development. Based on previous studies, we hypothesized that absorbance peak areas related to simple plant-derived OM (S-POM) would decrease with increasing soil formation as binding sites for minerals become increasingly weathered and the formation of OMAs are reduced. Consequently, hence decreasing the protection of S-POM compounds from microbial degradation and transformation decreases. The peak areas of complex plant-derived OM (C-POM) were expected to increase with soil age due to preferential association with pedogenic iron oxides (Hall et al., 2016; Zhao et al., 2016; Huang et al., 2019). Finally, MOM was expected to strongly increase with soil age since microbial uptake of OM and the subsequent stabilization in soils leads to an increasing share of microbial-derived SOM (Cotrufo et al., 2013; Cotrufo et al., 2015).

2 Material and methods

2.1 Site description

These present study links information on soil mineralogy and texture (Doetterl et al. 2018) with proxies for microbial transformation and SOM composition to derive a better understanding of long-term SOM dynamics along weathering gradients.

The study area is located in the California Central Valley (Merced County, CA, USA), where granitic debris with a minor share of mafic minerals from the Sierra Nevada foothills was deposited on alluvial terraces of the Merced River during interglacial periods (Harden, 1987; White et al., 1996; White et al., 2005). The alluvial deposits cover a temporal range of 3 million years, with the youngest terrace only 100 years old (Harden, 1987; Doetterl et al., 2018). We assume that the soil age corresponds to the age of the terrace depositions. The present climatic conditions ~~are homogeneous~~ across the study region are semiarid, being semiarid with a mean annual temperature of 16.3 °C and a mean annual precipitation of 315 mm (Reheis et al., 2012). ~~The vegetation cover is uniform along the chronosequence.~~ On the flat, plateau-like terraces, extensive, unfertilized rangeland dominates, which is not affected by wildfires. The vegetation cover is uniform along the chronosequence, consisting of annual Mediterranean grasslands ~~vegetation~~, with common species including *Bromus mollis*, *Festuca spp.* (grasses), *Erodium spp.* (forbs), and legumes (*Trifolium spp.*) (Jones and Woodmansee, 1979).

2.2 Soil sampling

Soil samples were collected in December 2013 from 1 m³ soil pits located within a circular area with a diameter of approximately 40 km in the North of Merced County. ~~Soil samples were collected in December 2013 within a diameter of approximately 40 km in the North of Merced County from 1 m³ soil pits (see map in~~ Fig. 1). The terraces are named based on different ~~quaternary glacial~~ periods that led to the alluvial deposition (Harden, 1987). The two youngest terraces are named Post-Modesto (PM) 24II (0.1 kyrs) and Post-Modesto (PM) 22 (3 kyrs). The intermediate terrace Modesto 2.4 m was deposited between 8 to 30 kyrs (Ø 19) ago. The two oldest terraces are Riverbank deposits (from 260 to 330 kyrs (Ø 295) ago) and Chinahat (3000 kyrs old deposits). In each ~~Per~~ terrace one plot was sampled and three field replicates were taken per pedogenic horizon (Doetterl et al., 2018). Yet, for the youngest 0.1 kyrs terrace, soils were only taken to a depth of 30 cm and in the case of the intermediate Modesto 2.4 m terrace, soil samples were taken from three different soil pits. To convert the pedogenic horizons to homogeneous depth classes (0-10 and 10-30 cm), weighted arithmetic means were calculated based on the contribution of each pedogenic horizon to the respective depth class. All soils were classified as chromic Luvisols except for the 3 kyrs terrace (PM 22) which was classified as a dystric Fluvisol. The total sample set was comprised of 30 observations.

2.3 Soil analysis

Doetterl et al. (2018) quantified elemental composition, pedogenic oxides, soil pH, ~~and~~ cation exchange capacity (CEC), and soil texture. Elemental composition of the soil samples was determined using inductively coupled plasma-atomic emission

spectrometry (ICP-AES) after borate fusion (Chao and Sanzolone, 1992). Extraction of pedogenic organo-mineral associations and oxy-hydroxides was done using dithionite-citrate-bicarbonate (DCB) at pH 8 (Mehra and Jackson, 1960). The extracted pedogenic oxides (Fe_{DCB} , Al_{DCB}) were then quantified using ICP-AES and serve as a measure of how many Fe- and Al-bearing phases formed during soil pedogenesis. The degree of mineral weathering along the chronosequence was assessed based on successive depletion and/or accumulation of geochemical components. For instance, the $Fe_{total}:Si_{total}$ ratio indicates how the mostly pedogenically formed Fe_{total} relates with Si_{total} , an element that abounds in the felsic parent material and accumulates in the semi-arid environment of the study area (White et al., 2005). Hence, the ratio decreases with increasing soil weathering. Similarly, the Ti:Zr ratio indicates the accumulation of Ti (constituent of many minerals) through mineral weathering relative to Zr (amount largely determined by the parent material). In addition, the increasing share of organo-mineral associated Fe (Fe_{DCB}) and Al (Al_{DCB}) was assessed relative to Fe_{total} ($Fe_{total}:Fe_{DCB}$) and Al_{total} , respectively.

Soil pH was averaged from two measurements, after 30 min and 24 h, in 0.01 M $CaCl_2$ with a glass electrode. The potential CEC was measured as the NH_4^+ exchanged after saturating cation exchange sites with aluminium acetate with 2 M KCl buffered at pH 7. The share of base saturation (B_{sat}) was calculated as the availability of all base cations (K, Na, Mg, Ca) relative to the potential CEC. Soil texture was analysed by Doetterl et al. (2018) with a Mastersizer 2000 laser diffraction particle size analyser (Malvern Instruments). Clay ($< 2 \mu m$), silt (2-63 μm), and sand (63 $\mu m - 2 mm$) were differentiated based on the WRB classification (WRB 2014). In silty soils, clay is under- and silt is overestimated due to the planar geometry of clay minerals (Beuselinck et al., 1998). Therefore, correction factors (see Eq. 1) were employed that correct the percentage of silt based on previous studies (Beuselinck et al., 1998; Miller and Schaetzl, 2012):

$$\% \text{ silt} = 100 - (\% \text{ estimated clay} + \% \text{ estimated sand}) \quad (1)$$

~~To prevent potential underestimation of clay in silty soils, correction factors were used (Beuselinck et al., 1998; Miller and Schaetzl, 2012):~~

Soil samples were ground in a ball mill (8000M Mixer/Mill, with a 55 mL tungsten carbide vial, SPEX SamplePrep, LLC, Metuchen, NJ, USA) previous-prior to SOM analysis. To assess the degree of microbial transformation of SOM, we quantified the stable isotope ratios using an elemental combustion system (Costech ECS 4010 CHNSO Analyzer, Costech Analytical Technologies, Valencia, CA, USA) that was interfaced with an isotope ratio mass spectrometer (DELTA V Plus Isotope Ratio Mass Spectrometer, Thermo Fisher Scientific, Inc., Waltham, MA, USA). The stable isotope values were complemented with total C values taken from Doetterl et al. (2018). Stable isotope values for $\delta^{13}C$ and $\delta^{15}N$ were calculated as the ratio of ^{13}C over ^{12}C and ^{15}N over ^{14}N (R_{sample}) relative to the Vienna Pee Dee Belemnite (VPDB) standard for $\delta^{13}C$ and relative to atmospheric N_2 for $\delta^{15}N$ ($R_{standard}$). Calculation followed Araya et al. (2017) (see Eq. 2):

$$\delta [\text{‰}] = \frac{(R_{\text{sample}} - R_{\text{standard}})}{R_{\text{standard}}} \times 1000 \quad (2) \delta [\text{‰}] = [(R_{\text{sample}} - R_{\text{standard}}) / R_{\text{standard}}] \times 1000$$

The spectroscopic analysis was carried out with a Bruker IFS 66v/S Vacuum FT-IR spectrometer (Bruker Biosciences Corporation, Billerica, MA, USA) to collect diffuse mid-infrared reflectance with a wavenumber range from 4000 to 400 cm⁻¹ (2500-25000 nm wavelength). In our analysis, 100 co-added scans were performed on each ground sample and averaged for further analysis. Spectra were normalized with the Standard Normal Variate (SNV) method for scatter correction, and a potassium-bromide (KBr) background for baseline correction. Subsequently, absorbance peak areas were integrated using a local baseline defined as a straight line connecting the absorbances at the upper and lower wavenumber limits of each functional group (Demyan et al., 2012). Negative peak areas were attributed to noise due to low C stocks and not to excessive signal strength, as they only occurred in the subsoil. To account for potential variation in signal strength due to varying C stocks, the peak areas were divided by the respective C stocks. The treatments of the spectra were performed using the OPUS software (Version 7.5.18; Bruker Optik GmbH, Ettlingen, Germany).

We differentiated three functional groups, based on extensive previous research and reviews (Demyan et al., 2012; Vranova et al., 2013; Parikh et al., 2014; Ryals et al., 2014; Viscarra Rossel et al., 2016; Fissore et al., 2017; Hall et al., 2018): aliphatic C-H bonds, aromatic C=C bonds and C=O bonds (see Fig. 2). These three functional groups are known to be indicative of three groups of SOM compounds with strongly differing chemical properties, and consequently differing bioavailability to microorganisms in soil systems (see Table 1). The wavenumber ranges centered at 2925 cm⁻¹ (2976-2898 cm⁻¹) and 2850 cm⁻¹ (2870-2839 cm⁻¹) are attributed to antisymmetric and symmetric aliphatic C-H stretching (Parikh et al., 2014) and represent simple plant-derived organic compounds (S-POM), e. g. originate from leaf compounds (i.e. waxes) as well as certain organic acids that are secreted by plant roots (i.e. citrate and oxalate) (Vranova et al., 2013). The second wavenumber range, located at 1512 cm⁻¹ (1550-1500 cm⁻¹), represents aromatic C=C compounds (Parikh et al., 2014). This functional group is related to lignin-derived, complex plant-derived compounds (C-POM) present in lignin constituents of wooden plant parts and aromatic organic acids of root exudates (Ryals et al. 2014). A large wavenumber range at 1620 cm⁻¹ (1660-1580 cm⁻¹) represents a carboxylic C=O stretch of amides, quinones and ketones, with possible shares of aromatic compounds (Parikh et al., 2014). This peak area is interpreted as microbially derived organic compounds (MOM) and jointly represents amides and quinones, which constitute microbial cell walls, and a ketone contribution attributed to long-chained lipids that can also be found in plant materials (Kögel-Knabner and Amelung, 2014). Wavenumber ranges that overlap with signals from mineral compounds, i.e. between 1400 to 400 cm⁻¹ (Parikh et al., 2014; Margenot et al., 2017) were excluded from our analysis.

2.4 Statistical analysis

Statistical analysis was carried out using R (Version 4.0.1, R Core Team, 2020). Two-way analysis of variance (ANOVA) was carried out to assess differences across soil age (0.1, 3, 19, 295, 3000 kyrs) and soil depth (topsoil: 0-10 and subsoil: 10-30

cm) to identify significant trends of bulk SOM composition parameters ($n = 30$). ~~The significance level of the ANOVA results was at $p < 0.05$. For the mineralogy and texture data taken from Doetterl et al. (2018) no ANOVA was carried out due to the low number of observations ($n = 10$).~~ Prior to the ANOVA, residuals were tested for normality with a Shapiro-Wilk test and the homogeneity of variances were checked with a Levene's test. We used Tukey's Honest Significant Difference (HSD) as a post-hoc test for pairwise comparison of homogeneous subgroups across soil ages. For the mineralogy and texture data taken from Doetterl et al. (2018) no ANOVA was carried out due to the low number of observations ($n = 10$).

~~Due to the size of the dataset ($n = 30$),~~ Linear models were formulated to explain the influence of mineralogy and texture variables on the SOM composition (dependent variables: C:N ratio, $\delta^{15}\text{N}$, $\delta^{13}\text{C}$, S-POM, C-POM, MOM) in dependence of soil age and soil depth. We controlled for multicollinearity among all variables by calculating variance-inflation factors (VIF) and excluded all variables with VIFs above 5 (Kuhn, 2020). VIFs quantify the ~~strength of correlation between explanatory variables~~ collinearity of a variable with the model (Fox and Monette, 1992; Fox and Weisberg, 2019). The VIF of each variable is ~~was~~ computed as following (James et al., 2013) (Eq. 3):

$$VIF(\hat{\beta}) = \frac{1}{1-R^2_{X_j|X_j}} \quad (3)$$

~~Out of the variables presented in Table 2 and 3, the $\text{Fe}_{\text{total}}:\text{Si}_{\text{total}}$ ratio, clay content, Fe_{DCB} , and Al_{DCB} were selected as explanatory variables as their inflation factor was below 5. Based on these variables, linear least squares regressions without interaction terms or non-linear effects were calculated to explain SOM properties (C:N ratio, $\delta^{13}\text{C}$, $\delta^{15}\text{N}$, S-POM, C-POM, and MOM). To assess the variable importance of the model parameters we used the absolute t-values which are calculated by dividing the parameter estimate (β_j) by the standard error of estimation (SE_j) (James et al., 2013; Kuhn, 2020). The t-value is a measure to determine the effect that each parameter makes~~ has ~~on the regression slope (Grömping, 2015). To give information on the significance of the impact, we added the p-value attributed to each predictor (Bring, 1996). The values of the t statistic were used as a measure of variable importance for each model parameter (Kuhn, 2020).~~ The goodness of model fit was quantified with the R^2 value. The root mean squared error (RMSE), as a measure of prediction error, and the mean absolute error (MAE), as a measure of model bias, were ~~was~~ quantified as a measure of deviation by a Monte-Carlo cross-validation following a leave-one-group-out principle. Thus, the RMSE and MAE were ~~was~~ calculated as the difference between predicted values based on a randomly selected training set (80 % of the observations) in relation to a randomly selected validation set (20 % of the observations) and relative to the sample size. The RMSE, the MAE, as well as the R^2 values were averaged and respective standard deviations were calculated based on 100 iterations of the cross-validation. In addition, we calculated the relative RMSE (rRMSE) and relative MAE (rMAE). They were calculated as the quotient of the RMSE and the mean of the response variable and multiplied by 100 (to get percentages).

3 Results

3.1 Changes in soil properties and SOM composition along the chronosequence

215 With increasing soil age, the soil mineral matrix was progressively weathered. Weathering and leaching of cations were reflected in downward decreasing trends led to a reduction of the CEC of 70 % from 15.2 to 4.5 in 0-10 cm depth (difference between youngest (0.1 kyrs) and oldest (3000 kyrs) terrace) in 0-10 cm and 85 % and from 14.2 to 2.1 in 10-30 cm depth (see Table 2). Similarly, which was also accompanied by a steady decrease in soil pH showed a trend tendencies to decrease from 6.8 to 4.7 in 0-10 cm and 6.8 to 4.3 in 10-30 cm depth along the chronosequence (see Table 2 and 3). Yet, the gradient observed for CEC and soil pH was not found in base saturation (B_{sat}) values which did not. B_{sat} showed no any clear trend pattern with 220 increasing soil age but were consistently higher in the 10-30 cm compared to 0-10 cm depth (except for the youngest 0.1 kyrs terrace). We observed/registered/identified a strong increase an increase by 63 % of Si_{total} from 241.5 g/kg to 393.4 g/kg in 0-10 cm and by 39 % from 280.3 to 389.4 g/kg in the 10-30 cm depth with increasing soil age (see Table 2). Al_{total} and Fe_{total} contents showed the opposite trend, decreasing ged with soil age in both depths (see Table 2). However, this decreasing trend was not displayed in the fractions of DCB-extractable Al (Al_{DCB}) and Fe (Fe_{DCB}) (see Table 2). While Al_{DCB} stagnated along 225 the age gradient at values ranging from 0.7 to 1.3 g/kg in 0-10 cm depth and 0.6 to 1.4 g/kg in 10-30 cm depth, Fe_{DCB} exhibited an increasing pattern trend in both depths. In 0-10 cm depth the values increased from 6.2 to 13.6 g/kg and in 10-30 cm depth from 6.1 to 13.5 g/kg. The higher Fe_{DCB} values among the DCB-extracted pedogenic oxides reflects the high potential of Fe to be quantitatively important for SOM binding even increased by 54 %. The $\text{Fe}_{\text{total}}:\text{Fe}_{\text{DCB}}$ ratio showed highest values in the soils of the 19 kyrs terrace (7.6 in 0-10 cm and 6.4 in 10-30 cm depth) (see Table 2). The and $\text{Al}_{\text{total}}:\text{Al}_{\text{DCB}}$ ratios were was highest in 230 soils of the 295 kyrs terrace with values of 88.5 in 0-10 cm depth and 106.8 in 10-30 cm depth (see Table 2), highest at intermediate soil development stages. Across all ages and both depths, Fe_{DCB} was the largest fraction of DCB-extracted pedogenic oxides, indicating the high potential of Fe to be quantitatively important for SOM binding (see Table 2 and 3).

Soil texture showed no clear patterns with soil age, but instead differed significantly between the 0-10 and 10-30 cm depths (see Table 2), however there were clear differences between soil depths. Except for the youngest terrace, silt and clay fractions 235 were more abundant in 10-30 cm depth, while the proportion of sand was mostly lower relative to the 0-10 cm depth.

Overall, bulk total C decreased significantly with soil depth (ANOVA results were significant at $p < 0.05$), and with soil age in the 0-10 cm depth (bulk C by 81 %) (see Fig. 3a). However, the decrease was not linear and the highest value C stock was measured but peaked at 3 kyrs ($3.6 \text{ kg/m}^2 \text{ C}$; see Fig. 3a). Furthermore, the C:N ratio was in general lower in 10-30 cm depth and in the 19, 295, and 3000 kyrs old soils compared to the 0.1 and 3 kyrs old soils (but did not show a clear trend with 240 increasing soil age) (see Fig. 3b). In contrast, $\delta^{13}\text{C}$ values showed no clear significant pattern with soil age but increased with soil depth (see Fig. 3c). The $\delta^{15}\text{N}$ values increased significantly with soil age but showed no significant difference from 0-10 to 10-30 cm depth (see Fig. 3d). Similarly, the peak areas of S-POM was/were significantly lower in the 10-30 cm depth and remained stable with increasing soil age (see Fig. 4a). Conversely, peak areas related to C-POM and MOM significantly

increased with ~~increasing~~ age in 0-10 cm depth (~~C-POM by 94 %; MOM by 90 %~~) and 10-30 cm depth (~~C-POM by 87 %; MOM by 66 %~~). Moreover, ~~higher~~ peak areas were significantly higher in 10-30 cm ~~suggest a positive trend with soil depth~~ (see Fig. 4b and 4c).

3.2 Link between soil geochemistry and SOM composition

The DRIFTS peak areas related to S-POM decreased significantly with soil depth while the C-POM and MOM signals rose significantly with increasing soil age and soil depth (see Fig. 4). This raised the question whether there were identifiable soil properties driving the relative changes of S-POM, C-POM, and MOM. Therefore, we used a modelling approach to predict bulk SOM composition using the soil mineralogy and texture parameters which were not affected by multicollinearity (see Methods). In Table 43, the mean model fit (RMSE and R²), respective relative measures (rRMSE, rMAE), and variable importance coefficients are presented based on ~~the 100 iterations of~~ the cross-validated results of the linear models with randomly split/divided different ~~random~~ training and control sets (see Methods). ~~A strong relationship between the variables related to the mineral matrix, soil texture and SOM composition could be observed.~~

The ~~most important variable explaining the~~ C:N ratio was best explained by the Fe_{total}:Si_{total} ratio which was the most important variable contributing significantly to the regression slope ($p < 0.01$; see Table 43). However, the R² showed high variability and was comparatively overall low in relation to the other models (R²: 0.32 mean \pm 0.27 S.D.). The rRMSE of 17.9 % and the rMAE of 16.1 % indicated a good prediction error compared to the other models (see Table 3). The $\delta^{15}\text{N}$ values were most influenced by clay content, the Fe_{total}:Si_{total} ratio, and Al_{DCB}. ~~However, despite the high model fit, no model parameter was significant, was high compared to the C:N ratio model.~~ Similar results were obtained for the R² values of $\delta^{13}\text{C}$ values. ~~However, in this model all parameters were significant ($p < 0.001$)~~ Yet, and based on the absolute values of the variable importance coefficients, Fe_{DCB}, the Fe_{total}:Si_{total} ratio, and clay were as more important than Al_{DCB} (see Table 3). The rRMSE and rMAE were slightly higher for $\delta^{15}\text{N}$ compared to the C:N ratio model (rRMSE: 24.2 %; rMAE: 20.3 %) and low for $\delta^{13}\text{C}$ (rRMSE: -2.2 %; rMAE: -2.2 %). ~~Regarding the~~ The most important variables explaining the peak areas related to S-POM, the most important significant variable was clay ($p < 0.01$; see Table 3), were Al_{DCB}, Fe_{DCB}, and the Fe_{total}:Si_{total} ratio (see Table 4). Yet, the explained variance was low and had a high standard deviation variable (R²: 0.39 \pm 0.33). This is also reflected in a high rRMSE and rMAE of > 100 % (see Table 3). Conversely, the linear models explaining the variance of the peak areas linked to C-POM and MOM had high R² values (R²: 0.78 \pm 0.10 and 0.57 \pm 0.27, respectively) indicating a good fit. In both cases, clay content was the only significant model parameter ($p < 0.01$). ~~Despite the high variable importance of the~~ The Fe_{total}:Si_{total} ratio in the C-POM model, this parameter was not significant (see Table 3). The rRMSE (C-POM: 56.3 %, MOM: 61.7 %) and rMAE (C-POM: 45.8 %; MOM: 55.1 %) were high in both cases, followed by clay content contributed most to the model fit of the C-POM response variable. The clay content followed by Fe_{DCB} were the most important predictors of the MOM peak area.

Our study assessed to what extent SOM composition changes as driven by soil weathering. We found that soil mineralogical and texture properties were able to explain a large part of variance in SOM composition parameters (Table 43). SOM was increasingly processed as indicated by a significant decrease of the C:N ratio, $\delta^{13}\text{C}$, and $\delta^{15}\text{N}$ over time and significant decreases of $\delta^{13}\text{C}$ with soil depth. These developments were accompanied by significant increases of the ~~which went along~~ ~~with increasing~~ peak areas related to complex plant-derived OM (C-POM) and microbial derived OM (MOM), and constant peak areas related to simple plant-derived OM (S-POM) (see Fig. 5). This suggests that changes in soil mineralogy following weathering may likely exert control on SOM composition.

4.1 Assessing chemical alteration of soil mineralogy, texture, and SOM composition over time and depth

Older soils are increasingly weathered and soil fertility decreases, as indicated by the lower soil pH and CEC (see Table 2 ~~and~~ 32). Further, the increasing dominance of Si with ongoing mineral weathering indicates increasing amounts of low reactive clay-sized silicates, i.e. kaolinite, which offer less binding sites to SOM (White et al., 2005). At the same time, significantly lower total C in strongly weathered soils were accompanied by an increasing trend-amounts of pedogenic iron oxides, i.e. Fe_{DCB} that likely contributed to the unaltered base saturation values. Similar effects were observed in previous soil chronosequence studies, highlighting the importance of iron-bearing mineral phases for SOM stabilization in strongly weathered soils (Chorover et al., 2004; Mikutta et al., 2009). In this study, the increasing trends in pedogenic iron oxides co-varied with proxies that indicate increasingly stabilized and microbially transformed SOM (decreasing C:N ratio, increasing $\delta^{13}\text{C}$ and $\delta^{15}\text{N}$ values) and a shift towards a C-limited soil environment (Coyle et al., 2009; Cotrufo et al., 2021). The stronger microbial-derived origin of SOM is reflected in the increasing $\delta^{13}\text{C}$ and $\delta^{15}\text{N}$ values that develop due to isotopic discrimination of microorganisms against heavier ^{13}C and ^{15}N (Dijkstra et al., 2006; Dijkstra et al., 2008; Kramer et al., 2017).

Soil fertility and SOM stabilization capacity of soils decreased along the chronosequence, thus leading to lower total C stocks on old terraces and stronger signs of microbially transformed SOM following reduced C input (Doetterl et al., 2018). Additionally, we observed significant changes in the peak areas of different functional groups of different origins and complexity regarding their chemical structures. While peak areas of simple plant-derived OM (S-POM) were less affected over time but significantly decreased with depth, peak areas of microbial-derived (MOM) and complex plant-derived OM (C-POM) significantly increased over time and with depth (see Fig. 4). We related S-POM to aliphatic compounds from litter and/or root exudates, C-POM compounds to aromatic structures of aboveground woody debris and/or aromatic root constituents, and MOM to long-chained lipids of predominantly microbial origin (see Table 1).

Throughout the quaternary period, the climate and vegetation were variable undoubtedly varied. Nevertheless, still, in contrast to our expectation, we found that S-POM did not decrease along the chronosequence, thus indicating ~~as the vegetation~~

305 ~~provided~~ steady supply by above- (light fraction of litter compounds) and belowground input (low-molecular weight root exudates, Nardi et al., 2005) particularly in the topsoil layer. The ~~significant~~ ~~decreasing peak areas of S-POM~~ with depth might be related to a lower stabilization potential of aliphatic organic acids with increasing soil depth (Vranova et al., 2013). Yet, it is noteworthy that below the main rooting zone (> 16 cm depth) increases of aliphatic compounds have been observed in similar grassland soils which was explained by increasing stabilization on mineral surfaces (Feng et al., 2007). The latter is
310 further supported by the high affinity of S-POM, in particular citrate and oxalate, to bind with Fe and Al oxides (Fe_{DCB} ~~tended to increase~~ with soil age) in acidic soils (Clarholm et al., 2015). The ~~relative-significant~~ increase of MOM peak areas in parallel to the constant S-POM peak areas along the chronosequence could indicate that an increasing fraction of microbially processed and transformed OM gains importance in bulk SOM with soil age (Feng et al., 2007). Previous studies showed a strong correlation between the MOM peak area and organo-mineral associations (Kaiser et al., 2007; Demyan et al., 2012;
315 Kaiser et al., 2012). Thus, the observed increases in our study hint towards an increasing importance of OMAs with progressing soil weathering. C-POM signals, interpreted as lignin-compounds from woody plant parts, behaved similarly to MOM and ~~significantly~~ increased with soil age and depth. In grassland soils, increases of signals related to lignin compounds with depth were explained by the increasing dominance of root-derived OM input in subsoils (Feng et al., 2007). Yet, increases in lignin compounds were also observed following a preferential association with iron oxides which is supported by the increase of
320 pedogenic Fe_{DCB} with soil age (Hall et al., 2016; Zhao et al., 2016) as well as kaolinite which is supported by the increasing clay contents in our samples with soil depth (Li et al., 2019).

4.2 Mineralogical control of SOM dynamics over geological time

As indicated above, the changes in the degree of decomposition (as indicated by the C:N ratio, $\delta^{13}\text{C}$, and $\delta^{15}\text{N}$) and SOM composition (peak areas of S-POM, MOM, and C-POM) must be contemplated in the light of simultaneously occurring
325 changes of the mineral matrix along the chronosequence. Therefore, ~~in this section here~~ we discuss to which extent the relationship between soil mineralogy, texture, and SOM (de-)composition is reflected in linear models and how these findings can be embedded in our current understanding of SOM dynamics.

The properties related to SOM decomposition showed differences in the model fit (see Table 4.3). The C:N ratio showed the lowest model fit of all SOM composition properties. Low and variable R² values highlighted that the mineral matrix did not
330 strongly affect the C:N ratio of bulk SOM even though SOM was progressively decomposed with increasing soil age. The only variable that contributed significantly to the explanation of the C:N ratio was the Fe_{total}:Si_{total} ratio. The ~~decreasing trend~~ of the Fe_{total}:Si_{total} ratio with soil age indicated that during soil weathering processes, low reactive silicates, i.e. quartz, or 1:1 layer type clay minerals (kaolinite), abound (White et al., 2005). The second most important predictor variable, Fe_{DCB}, reflects an increasing importance of pedogenic iron oxides in SOM stabilization as these compounds retain very high reactive surface

335 areas (Kleber et al., 2021). Our findings show that the properties of the mineral matrix play a subordinate role in shaping the C:N ratio which is more strongly driven by the increasing microbial origin of the SOM (Sollins et al., 2009).

In contrast to the C:N ratio, linear models with $\delta^{13}\text{C}$ and $\delta^{15}\text{N}$ values as response variables showed a good model fit ($R^2 > 0.60$, (see Table 43). The $\delta^{13}\text{C}$ values were strongly related to Fe_{DCB} , $\text{Fe}_{\text{total}}:\text{Si}_{\text{total}}$, and clay, while $\delta^{15}\text{N}$ values were explained by clay, $\text{Fe}_{\text{total}}:\text{Si}_{\text{total}}$, and Al_{DCB} (although not significantly). In both cases, the high importance of clay content as predictor supports empirical findings that SOM with a higher share of microbial-derived OM (high $\delta^{15}\text{N}$; high MOM signal) and increasingly decomposed OM (low C:N ratio; high $\delta^{15}\text{N}$, less negative $\delta^{13}\text{C}$) is predominantly found within the heavy (clay) fraction of soils (Conen et al., 2008; Sollins et al., 2009; Clemente et al., 2011; Lawrence et al., 2015). It has been previously demonstrated that SOM bound to iron oxides was enriched in $\delta^{13}\text{C}$ and exhibited more MOM (Zhao et al., 2016). Likely the imprint of $\delta^{13}\text{C}$ enrichment with increasing microbial transformation of the SOM manifested itself more clearly in bulk SOM as the overall C stocks decreased in the oldest soils (Yang et al., 2015).

Similar to the models explaining SOM decomposition variables, the linear models on DRIFTS peak areas had varying model fits (see Table 43). The model for S-POM had a lower model fit ($R^2 = 0.39$) compared to the models explaining C-POM and MOM ($R^2 = 0.78$ and 0.57 , respectively). In all models, the clay content was ~~a~~the key explanatory variable which hints at different behaviours in top- and subsoils as consistently higher shares of clay were found in the 10-30 cm depth (see Table 32). The fact that S-POM was ~~less-not significantly~~ influenced by the $\text{Fe}_{\text{total}}:\text{Si}_{\text{total}}$ ratio suggests that the contribution of S-POM to OM is less related to weathering-induced changes of the mineral matrix, but rather determined by above- and belowground vegetation input, i.e. through litter components or root exudates (Vranova et al., 2013; Mueller et al., 2013). Lower signals of S-POM in subsoils compared to topsoils (see Fig. 4) indicate that the mineral stabilization of S-POM compounds in subsoils is lower or that S-POM compounds are less abundant at these depths (Vranova et al., 2013). Still, the ~~relativehigher~~ variable importance of Al_{DCB} and Fe_{DCB} to explain S-POM ~~potentially~~ indicates that certain compounds, likely aliphatic organic acids derived from root exudates, are preferentially attached to minerals (Clarholm et al., 2015).

In the case of C-POM, the decreasing $\text{Fe}_{\text{total}}:\text{Si}_{\text{total}}$ ratio with increasing soil age ~~had the highest variable importance coefficient but was not significant to the model~~was the most important predictor. ~~The high variable importance coefficient is in line with other studies that found~~This supports the notion that functional groups that are considered chemically more complex (i.e. through an aromatic ring structure) ~~to be~~are increasingly stabilized relative to other functional groups, as soils become more weathered, ~~and~~ as overall SOM stocks deplete, ~~and along with reduced~~ protection through reactive mineral ~~surfaces declines~~ in strongly weathered soils (Angst et al., 2018). Lignin compounds represented by C-POM were shown to be better stabilized due to attachment on mineral surfaces, such as calcite (Grünewald et al., 2006), kaolinite (Li et al., 2019), as well as Fe oxides (Kramer et al., 2012; Hall et al., 2016; Zhao et al., 2016; Huang et al., 2019). Yet, the coefficients of variable importance of the C-POM model did not show a particular importance of Fe_{DCB} and Al_{DCB} (see Table 43). Potentially the more linear decrease of the $\text{Fe}_{\text{total}}:\text{Si}_{\text{total}}$ ratio might mask less ~~linear-consistent~~ increases of Fe_{DCB} or the varying behaviour of Al_{DCB} (see Table 2 ~~and~~

3) ~~Instead, e~~Clay content was the ~~second most important~~ only significant predictor, and it was previously shown that kaolinite accumulates in the mineral matrix with increasing soil age and depth along the present chronosequence (White et al., 2005). Hence, the mineral stabilization of C-POM in heavy soil fractions might be more strongly linked to the presence of clay minerals than iron oxides (Li et al., 2019; Grünewald et al., 2006).

The ~~peak areas related to MOM~~ most important predictors to explain the peak areas related to MOM were significantly explained by the clay content and Fe_{DCB} (see Table 4.3). ~~These predictors highlight the similarity of the MOM peak area with variables like $\delta^{13}\text{C}$ that are related to SOM decomposition~~ This is consistent with the significant model parameters for S-POM and C-POM. Both properties reflect the increasingly microbial derived imprint in the bulk SOM. The clay fraction is known to harbour the vast majority of soil microorganisms and to stimulate their activity (i.e. Stotzky and Rem, 1966; Sollins et al., 2009). Therefore, it is logical that the increasingly microbial derived imprint in the bulk SOM is significantly linked to the clay fraction. Our study is in line with these findings as MOM signals increased with increasing clay content. However ~~Further, the Fe_{DCB} parameter had a higher variable importance coefficient~~ the MOM peak also showed a strong link to Fe_{DCB} suggesting a link between ~~which might be linked to the~~ increasing importance of pedogenic iron oxides and MOM along the soil chronosequence. This might be caused by the increasing importance of metal surfaces in stabilizing bulk SOM, but also soil microorganisms or microbial necromass in particular (Kaiser et al., 1997, Zhao et al., 2016). Yet, these interpretations are more speculative due to the heterogeneity of soil microorganisms and the vast range of possible interactions requires further investigation.

5 Conclusion

The present observational study provides new information on qualitative changes of the SOM composition in relation to soil geochemical dynamics driven by mineral weathering from a soil chronosequence covering a gradient of 3 million years. With progressing soil development ~~As~~ SOM stocks decreased and, we observed an increasingly microbially transformed bulk SOM (lower C:N ratio, higher $\delta^{13}\text{C}$ and $\delta^{15}\text{N}$ values) ~~with progressing soil development~~. Simultaneously, the spectroscopic fingerprint of SOM (reflected in the peak areas related to S-POM, C-POM, and MOM) shifted, as exhibiting with increasing peak areas of structurally more complex compounds increased (C-POM and MOM). ~~We relate t~~ These qualitative changes in SOM composition co-occurred with ~~to~~ changes in the ~~of~~ soil geochemistry and texture induced by soil formation, ~~and suggest that e~~ Hence, changes in soil texture (clay content) and an increasingly kaolinite- and iron oxide-rich, strongly weathered mineral matrix might ~~discriminates~~ in favour of structurally more complex SOM compounds (C-POM and MOM). Our study shows that soil mineralogy plays an important role in shaping SOM composition during soil weathering across large timescales. We therefore recommend further studies to assess these trends link in contrasting soil mineralogies or vegetation types, in order to gain a better understanding of how soil mineral matrix and C input related changes affect SOM composition across larger geographical areas.

Author contributions

AAB and SD designed the experiments. MM performed the measurements, analysed the data and wrote the manuscript. DW, GG, MG, and LS reviewed and edited the manuscript. LS created the map (Fig. 1). All authors contributed to writing the paper (Lead author: MM).

Competing interests

The authors declare that they have no conflict of interest.

Acknowledgements

This study was carried out with the financial support of the Bavaria California Technology Center (BaCaTeC) (Project 22, 2016-1). We thank the working group of Asmeret A. Berhe for logistic help and support in the laboratory.

References

- Angst, G., Nierop, K. G. J., Angst, Š., and Frouz, J.: Abundance of lipids in differently sized aggregates depends on their chemical composition, *Biogeochemistry*, 140, 111–125, <https://doi.org/10.1007/s10533-018-0481-7>, 2018.
- Araya, S. N., Fogel, M. L., and Berhe, A. A.: Thermal alteration of soil organic matter properties: A systematic study to infer response of Sierra Nevada climosequence soils to forest fires, 3, 31–44, <https://doi.org/10.5194/soil-3-31-2017>, 2017.
- Austin, A. T. and Vitousek, P. M.: Nutrient dynamics on a precipitation gradient in Hawai'i, *Oecologia*, 113, 519–529, <https://doi.org/10.1007/s004420050405>, 1998.
- Bailey, V. L., Hicks Pries, C., and Lajtha, K.: What do we know about soil carbon destabilization?, *Environ. Res. Lett.*, 14, 083004, <https://doi.org/10.1088/1748-9326/ab2c11>, 2019.
- Baldock, J. A., Creamer, C., Szarvas, S., McGowan, J., Carter, T., and Farrell, M.: Linking decomposition rates of soil organic amendments to their chemical composition, *Soil Res.*, 59, 630–643, <https://doi.org/10.1071/SR20269>, 2021.
- Barré, P., Durand, H., Chenu, C., Meunier, P., Montagne, D., Castel, G., Billiou, D., Soucémarianadin, L., and Cécillon, L.: Geological control of soil organic carbon and nitrogen stocks at the landscape scale, *Geoderma*, 285, 50–56, <https://doi.org/10.1016/j.geoderma.2016.09.029>, 2017.
- Benner, R., Fogel, M. L., Sprague, E. K., and Hodson, R. E.: Depletion of C in lignin and its implications for stable carbon isotope studies, *Nature*, 329, 708–710, <https://doi.org/10.1038/329708a0>, 1987.
- Beuselinck, L., Govers, G., Poesen, J., Degraer, G., and Froyen, L.: Grain-size analysis by laser diffractometry: Comparison with the sieve-pipette method, 32, 193–208, [https://doi.org/10.1016/S0341-8162\(98\)00051-4](https://doi.org/10.1016/S0341-8162(98)00051-4), 1998.

- 425 Bradford, M. A., Wieder, W. R., Bonan, G. B., Fierer, N., Raymond, P. A., and Crowther, T. W.: Managing uncertainty in soil carbon feedbacks to climate change, *Nat. Clim. Chang.*, 6, 751–758, <https://doi.org/10.1038/nclimate3071>, 2016.
- [Bring, J.: A geometric approach to compare variables in a regression model. *The American Statistician*, 50, 57-62, 1996.](#)
- Brunn, M., Condrón, L., Wells, A., Spielvogel, S., and Oelmann, Y.: Vertical distribution of carbon and nitrogen stable isotope ratios in topsoils across a temperate rainforest dune chronosequence in New Zealand, *Biogeochemistry*, 129, 37–51, <https://doi.org/10.1007/s10533-016-0218-4>, 2016.
- 430 Bullen, T., White, A., Blum, A., Harden, J., and Schulz, M.: Chemical weathering of a soil chronosequence on granitoid alluvium: II. Mineralogic and isotopic constraints on the behavior of strontium, *Geochim. Cosmochim. Acta*, 61, 291–306, [https://doi.org/10.1016/S0016-7037\(96\)00344-4](https://doi.org/10.1016/S0016-7037(96)00344-4), 1997.
- Calderón, F. J., Reeves, J. B., Collins, H. P., and Paul, E. A.: Chemical Differences in Soil Organic Matter Fractions Determined by Diffuse-Reflectance Mid-Infrared Spectroscopy, *Soil Sci. Soc. Am. J.*, 75, 568–579, <https://doi.org/10.2136/sssaj2009.0375>, 2011.
- 435 Chao, T. T. and Sanzalone, R. F.: Decomposition techniques, *J. Geochemical Explor.*, 44, 65–106, [https://doi.org/10.1016/0375-6742\(92\)90048-D](https://doi.org/10.1016/0375-6742(92)90048-D), 1992.
- Chorover, J., Amistadi, M. K., and Chadwick, O. A.: Surface charge evolution of mineral-organic complexes during pedogenesis in Hawaiian basalt, *Geochim. Cosmochim. Acta*, 68, 4859–4876, <https://doi.org/10.1016/j.gca.2004.06.005>, 2004.
- 440 Clarholm, M., Skjellberg, U., and Rosling, A.: Organic acid induced release of nutrients from metal-stabilized soil organic matter - The unbutton model, *Soil Biol. Biochem.*, 84, 168–176, <https://doi.org/10.1016/j.soilbio.2015.02.019>, 2015.
- Clemente, J. S., Simpson, A. J., and Simpson, M. J.: Association of specific organic matter compounds in size fractions of soils under different environmental controls, *Org. Geochem.*, 42, 1169–1180, <https://doi.org/10.1016/j.orggeochem.2011.08.010>, 2011.
- 445 Conen, F., Zimmermann, M., Leifeld, J., Seth, B., and Alewell, C.: Relative stability of soil carbon revealed by shifts in $\delta^{15}\text{N}$ and C:N ratio, 5, 123–128, <https://doi.org/10.5194/bg-5-123-2008>, 2008.
- Cotrufo, M. F., Wallenstein, M. D., Boot, C. M., Deneff, K., and Paul, E.: The Microbial Efficiency-Matrix Stabilization (MEMS) framework integrates plant litter decomposition with soil organic matter stabilization: Do labile plant inputs form stable soil organic matter?, *Glob. Chang. Biol.*, 19, 988–995, <https://doi.org/10.1111/gcb.12113>, 2013.
- 450 Cotrufo, M. F., Soong, J. L., Horton, A. J., Campbell, E. E., Haddix, M. L., Wall, D. H., and Parton, W. J.: Formation of soil organic matter via biochemical and physical pathways of litter mass loss, *Nat. Geosci.*, 8, 776–779, <https://doi.org/10.1038/ngeo2520>, 2015.
- 455 Francesca Cotrufo, M., Lavelle, J. M., Zhang, Y., Hansen, P. M., Paustian, K. H., Schipanski, M., and Wallenstein, M. D.: In-N-Out: A hierarchical framework to understand and predict soil carbon storage and nitrogen recycling, *Glob. Chang. Biol.*, 27, 4465–4468, <https://doi.org/10.1111/gcb.15782>, 2021.

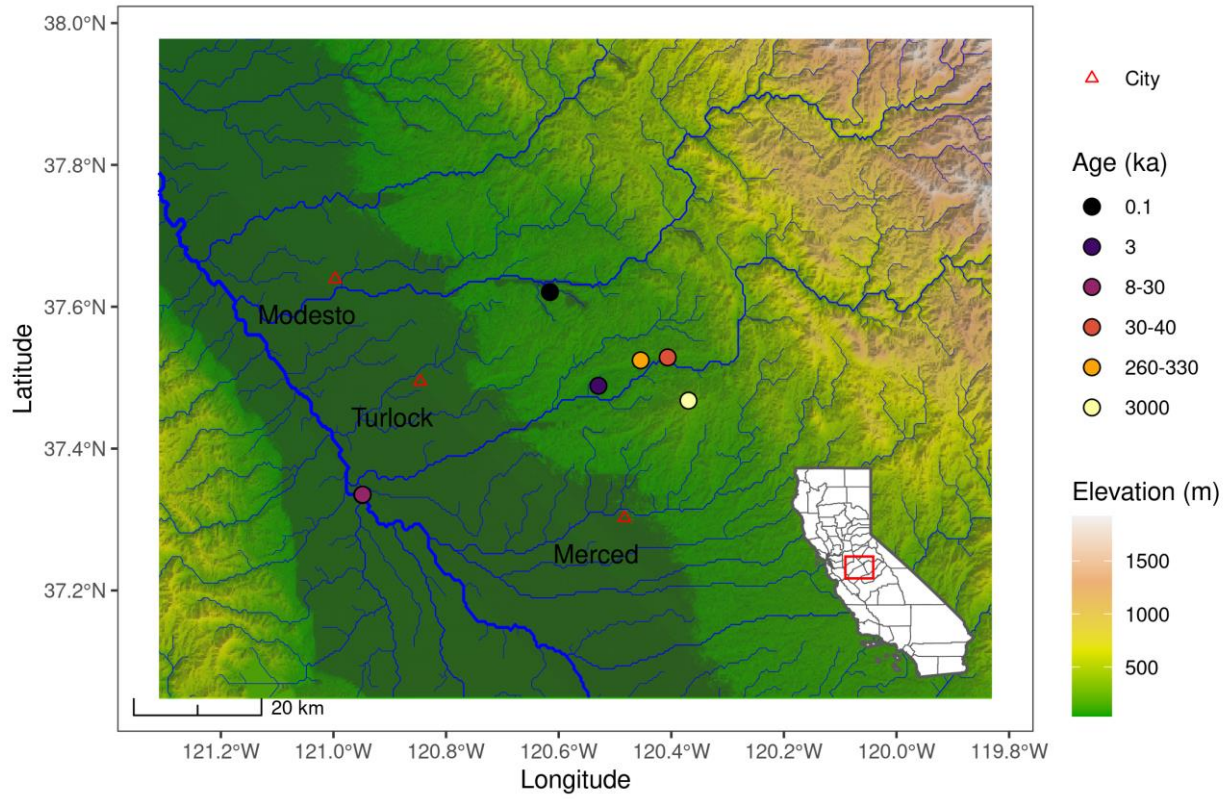
- 460 Coyle, J. S., Dijkstra, P., Doucett, R. R., Schwartz, E., Hart, S. C., and Hungate, B. A.: Relationships between C and N availability, substrate age, and natural abundance ^{13}C and ^{15}N signatures of soil microbial biomass in a semiarid climate, *Soil Biol. Biochem.*, 41, 1605–1611, <https://doi.org/10.1016/j.soilbio.2009.04.022>, 2009.
- Demyan, M. S., Rasche, F., Schulz, E., Breulmann, M., Müller, T., and Cadisch, G.: Use of specific peaks obtained by diffuse reflectance Fourier transform mid-infrared spectroscopy to study the composition of organic matter in a Haplic Chernozem, *Eur. J. Soil Sci.*, 63, 189–199, <https://doi.org/10.1111/j.1365-2389.2011.01420.x>, 2012.
- 465 Dijkstra, P., Ishizu, A., Doucett, R., Hart, S. C., Schwartz, E., Menyailo, O. V., and Hungate, B. A.: ^{13}C and ^{15}N natural abundance of the soil microbial biomass, *Soil Biol. Biochem.*, 38, 3257–3266, <https://doi.org/10.1016/j.soilbio.2006.04.005>, 2006.
- Doetterl, S., Berhe, A. A., Arnold, C., Bodé, S., Fiener, P., Finke, P., Fuchslueger, L., Griepentrog, M., Harden, J. W., Nadeu, E., Schnecker, J., Six, J., Trumbore, S., Van Oost, K., Vogel, C., and Boeckx, P.: Links among warming, carbon and microbial dynamics mediated by soil mineral weathering, *Nat. Geosci.*, 11, 589–593, <https://doi.org/10.1038/s41561-018-0168-7>, 2018.
- 470 ~~Durrer, A., Margenot, A. J., Silva, L. C. R., Bohannan, B. J. M., Nusslein, K., van Haren, J., Andreote, F. D., Parikh, S. J., and Rodrigues, J. L. M.: Beyond total carbon: conversion of amazon forest to pasture alters indicators of soil C cycling, *Biogeochemistry*, 152, 179–194, <https://doi.org/10.1007/s10533-020-00743-x>, 2021.~~
- Ellerbrock, R. H. and Gerke, H. H.: Characterizing organic matter of soil aggregate coatings and biopores by Fourier transform infrared spectroscopy, *Eur. J. Soil Sci.*, 55, 219–228, <https://doi.org/10.1046/j.1365-2389.2004.00593.x>, 2004.
- 475 Feng, X. and Simpson, M. J.: The distribution and degradation of biomarkers in Alberta grassland soil profiles, *Org. Geochem.*, 38, 1558–1570, <https://doi.org/10.1016/j.orggeochem.2007.05.001>, 2007.
- Fissore, C., Dalzell, B. J., Berhe, A. A., Voegtli, M., Evans, M., and Wu, A.: Influence of topography on soil organic carbon dynamics in a Southern California grassland, 149, 140–149, <https://doi.org/10.1016/j.catena.2016.09.016>, 2017.
- 480 Fox, J. and Monette, G.: Generalized collinearity diagnostics, *J. Am. Stat. Assoc.*, 87, 178–183, <https://doi.org/10.1080/01621459.1992.10475190>, 1992.
- Fox, J. and Weisberg, S.: *An R Companion to Applied Regression*, Third edit., SAGE, Thousand Oaks, 2019.
- ~~[Grömping, U.: Variable importance in regression models. *WIREs Comput Stat*, 7, 137-152. <https://doi.org/10.1002/wics.1346.2015>.](https://doi.org/10.1002/wics.1346.2015)~~
- 485 Grünewald, G., Kaiser, K., Jahn, R., and Guggenberger, G.: Organic matter stabilization in young calcareous soils as revealed by density fractionation and analysis of lignin-derived constituents, *Org. Geochem.*, 37, 1573–1589, <https://doi.org/10.1016/j.orggeochem.2006.05.002>, 2006.
- Hall, S. J., Silver, W. L., Timokhin, V. I., and Hammel, K. E.: Iron addition to soil specifically stabilized lignin, *Soil Biol. Biochem.*, 98, 95–98, <https://doi.org/10.1016/j.soilbio.2016.04.010>, 2016.
- 490 Hall, S. J., Berhe, A. A., and Thompson, A.: Order from disorder: do soil organic matter composition and turnover co-vary with iron phase crystallinity?, *Biogeochemistry*, 140, 93–110, <https://doi.org/10.1007/s10533-018-0476-4>, 2018.

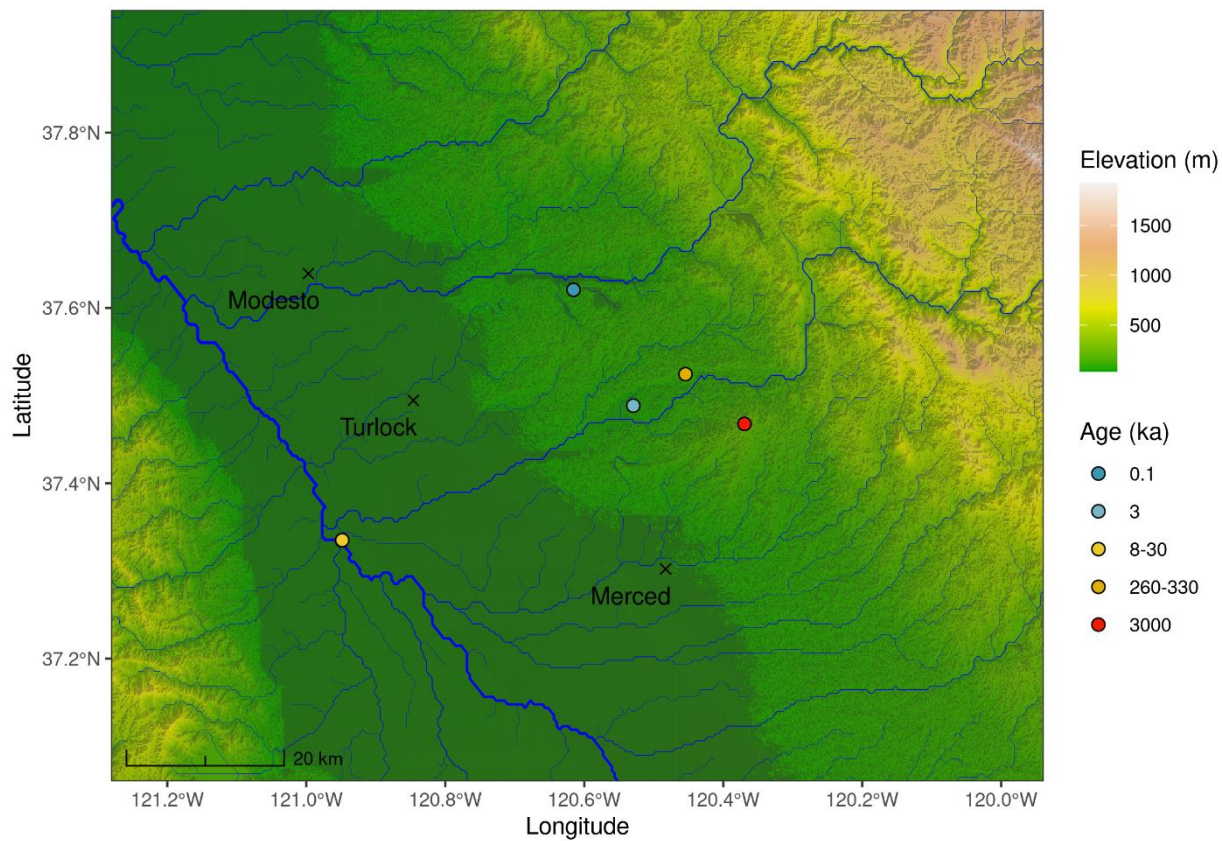
- Hall, S. J., Ye, C., Weintraub, S. R., and Hockaday, W. C.: Molecular trade-offs in soil organic carbon composition at continental scale, *Nat. Geosci.*, 13, 687–692, <https://doi.org/10.1038/s41561-020-0634-x>, 2020.
- Harden, J. W.: *Soils Developed in Granitic Alluvium near Merced, California*, U.S. Geological Survey, Denver, 1987.
- Huang, W., Hammel, K. E., Hao, J., Thompson, A., Timokhin, V. I., and Hall, S. J.: Enrichment of lignin-derived carbon in mineral-associated soil organic matter, *Environ. Sci. Technol.*, 53, 7522–7531, <https://doi.org/10.1021/acs.est.9b01834>, 2019.
- 495 [James, G., Witten, D., Hastie, T., Tibshirani, R.: An introduction to statistical learning. Springer: New York, Heidelberg, Dordbrecht, London, 2013.](#)
- Jobbágy, E. G. and Jackson, R. B.: The vertical distribution of soil organic carbon and its relation to climate and vegetation, *Ecol. Appl.*, 10, 423–436, [https://doi.org/10.1890/1051-0761\(2000\)010\[0423:TVDOSO\]2.0.CO;2](https://doi.org/10.1890/1051-0761(2000)010[0423:TVDOSO]2.0.CO;2), 2000.
- 500 Jones, M. B. and Woodmansee, R. G.: Biogeochemical cycling in annual grassland ecosystems, *Bot. Rev.*, 45, 111–144, <https://doi.org/10.1007/BF02860854>, 1979.
- Kaiser, K., Guggenberger, G., Haumaier, L., and Zech, W.: Dissolved organic matter sorption on subsoils and minerals studied by ¹³C-NMR and DRIFT spectroscopy, *Eur. J. Soil Sci.*, 48, 301–310, <https://doi.org/10.1111/j.1365-2389.1997.tb00550.x>, 1997.
- 505 Kaiser, M., Ellerbrock, R. H., and Gerke, H. H.: Long-term effects of crop rotation and fertilization on soil organic matter composition, *Eur. J. Soil Sci.*, 58, 1460–1470, <https://doi.org/10.1111/j.1365-2389.2007.00950.x>, 2007.
- Kaiser, M., Ellerbrock, R. H., Wulf, M., Dultz, S., Hierath, C., and Sommer, M.: The influence of mineral characteristics on organic matter content, composition, and stability of topsoils under long-term arable and forest land use, *J. Geophys. Res. Biogeosciences*, 117, 1–16, <https://doi.org/10.1029/2011JG001712>, 2012.
- 510 Khedim, N., Cécillon, L., Poulenard, J., Barré, P., Baudin, F., Marta, S., Rabatel, A., Dentant, C., Cauvy-Fraunié, S., Anthelme, F., Gielly, L., Ambrosini, R., Franzetti, A., Azzoni, R. S., Caccianiga, M. S., Compostella, C., Clague, J., Tielidze, L., Messenger, E., Choler, P., and Ficitola, G. F.: Topsoil organic matter build-up in glacier forelands around the world, *Glob. Chang. Biol.*, 27, 1662–1677, <https://doi.org/10.1111/gcb.15496>, 2021.
- 515 Kleber, M., Nico, P. S., Plante, A., Filley, T., Kramer, M., Swanston, C., and Sollins, P.: Old and stable soil organic matter is not necessarily chemically recalcitrant: Implications for modeling concepts and temperature sensitivity, *Glob. Chang. Biol.*, 17, 1097–1107, <https://doi.org/10.1111/j.1365-2486.2010.02278.x>, 2011.
- Kleber, M., Bourg, I. C., Coward, E. K., Hansel, C. M., Myneni, S. C. B., and Nunan, N.: Dynamic interactions at the mineral–organic matter interface, *Nat. Rev. Earth Environ.*, 2, 402–421, <https://doi.org/10.1038/s43017-021-00162-y>, 2021.
- 520 Kögel-Knabner, I. and Amelung, W.: Dynamics, Chemistry, and Preservation of Organic Matter in Soils, 157–215 pp., <https://doi.org/10.1016/B978-0-08-095975-7.01012-3>, 2014.
- Kögel-Knabner, I. and Amelung, W.: Soil organic matter in major pedogenic soil groups, *Geoderma*, 384, <https://doi.org/10.1016/j.geoderma.2020.114785>, 2021.

- 525 Kramer, M. G., Sanderman, J., Chadwick, O. A., Chorover, J., and Vitousek, P. M.: Long-term carbon storage through retention of dissolved aromatic acids by reactive particles in soil, *Glob. Chang. Biol.*, 18, 2594–2605, <https://doi.org/10.1111/j.1365-2486.2012.02681.x>, 2012.
- Kramer, M. G., Lajtha, K., and Aufdenkampe, A. K.: Depth trends of soil organic matter C:N and ¹⁵N natural abundance controlled by association with minerals, *Biogeochemistry*, 136, 237–248, <https://doi.org/10.1007/s10533-017-0378-x>, 2017.
- Kuhn, M.: caret: Classification and Regression Training, <https://cran.r-project.org/package=caret>, 2020.
- 530 Lal, R.: Soil carbon stocks under present and future climate with specific reference to European ecoregions, *Nutr. Cycl. Agroecosystems*, 81, 113–127, <https://doi.org/10.1007/s10705-007-9147-x>, 2008.
- Laub, M., Scott Demyan, M., Funkuin Nkwain, Y., Blagodatsky, S., Kätterer, T., Piepho, H. P., and Cadisch, G.: DRIFTS band areas as measured pool size proxy to reduce parameter uncertainty in soil organic matter models, 17, 1393–1413, <https://doi.org/10.5194/bg-17-1393-2020>, 2020.
- 535 Lavalée, J. M., Soong, J. L., and Cotrufo, M. F.: Conceptualizing soil organic matter into particulate and mineral-associated forms to address global change in the 21st century, *Glob. Chang. Biol.*, 26, 261–273, <https://doi.org/10.1111/gcb.14859>, 2020.
- Lawrence, C. R., Harden, J. W., Xu, X., Schulz, M. S., and Trumbore, S. E.: Long-term controls on soil organic carbon with depth and time: A case study from the Cowlitz River Chronosequence, WA USA, *Geoderma*, 247–248, 73–87, <https://doi.org/10.1016/j.geoderma.2015.02.005>, 2015.
- 540 Lehmann, J. and Kleber, M.: The contentious nature of soil organic matter, *Nature*, 528, 60–68, <https://doi.org/10.1038/nature16069>, 2015.
- Lehner, B., Verdin, K., Jarvis, A.: New global hydrography derived from spaceborne elevation data, *Eos, Transactions, AGU*, 89, 93-94, <https://doi.org/10.1029/2008EO100001>, 2008.
- 545 Li, F., Chang, Z., Khaing, K., Zhou, Y., Zhao, H., Liang, N., Zhou, D., Pan, B., and Steinberg, C. E. W.: Organic matter protection by kaolinite over bio-decomposition as suggested by lignin and solvent-extractable lipid molecular markers, *Sci. Total Environ.*, 647, 570–576, <https://doi.org/10.1016/j.scitotenv.2018.07.456>, 2019.
- Von Lützow, M., Kögel-Knabner, I., Ludwig, B., Matzner, E., Flessa, H., Ekschmitt, K., Guggenberger, G., Marschner, B., and Kalbitz, K.: Stabilization mechanisms of organic matter in four temperate soils: Development and application of a conceptual model, *J. Plant Nutr. Soil Sci.*, 171, 111–124, <https://doi.org/10.1002/jpln.200700047>, 2008.
- 550 Margenot, A. J., Calderón, F. J., Bowles, T. M., Parikh, S. J., and Jackson, L. E.: Soil organic matter functional group composition in relation to organic carbon, nitrogen, and phosphorus fractions in organically managed tomato fields, *Soil Sci. Soc. Am. J.*, 79, 772–782, <https://doi.org/10.2136/sssaj2015.02.0070>, 2015.
- Margenot, A. J., Calderón, F. J., Goyne, K. W., Mukome, F. N. D., and Parikh, S. J.: IR Spectroscopy, *Soil Analysis Applications, Encycl. Spectrosc. Spectrom.*, 2, 448–454, <https://doi.org/10.1016/B978-0-12-409547-2.12170-5>, 2017.
- 555 Mehra, O. P. and Jackson, M. L.: Iron Oxide Removal from Soils and Clay, in: *Proceedings of the National Conference on Clays and Clay Minerals*, 317–327, 1960.

- Mikutta, R., Kleber, M., Torn, M. S., and Jahn, R.: Stabilization of soil organic matter: Association with minerals or chemical recalcitrance?, *Biogeochemistry*, 77, 25–56, <https://doi.org/10.1007/s10533-005-0712-6>, 2006.
- Mikutta, R., Schaumann, G. E., Gildemeister, D., Bonneville, S., Kramer, M. G., Chorover, J., Chadwick, O. A., and Guggenberger, G.: Biogeochemistry of mineral-organic associations across a long-term mineralogical soil gradient (0.3-4100 kyr), Hawaiian Islands, *Geochim. Cosmochim. Acta*, 73, 2034–2060, <https://doi.org/10.1016/j.gca.2008.12.028>, 2009.
- 560
- Miller, B. A. and Schaetzl, R. J.: Precision of Soil Particle Size Analysis using Laser Diffractometry, *Soil Sci. Soc. Am. J.*, 76, 1719–1727, <https://doi.org/10.2136/sssaj2011.0303>, 2012.
- Mueller, K. E., Eissenstat, D. M., Müller, C. W., Oleksyn, J., Reich, P. B., and Freeman, K. H.: What controls the concentration of various aliphatic lipids in soil?, *Soil Biol. Biochem.*, 63, 14–17, <https://doi.org/10.1016/j.soilbio.2013.03.021>, 2013.
- 565
- Nardi, S., Tosoni, M., Pizzeghello, D., Provenzano, M. R., Cilenti, A., Sturaro, A., Rella, R., and Vianello, A.: Chemical Characteristics and Biological Activity of Organic Substances Extracted from Soils by Root Exudates, *Soil Sci. Soc. Am. J.*, 69, 2012–2019, <https://doi.org/10.2136/sssaj2004.0401>, 2005.
- Nunan, N., Lerch, T. Z., Pouteau, V., Mora, P., Changey, F., Kätterer, T., Giusti-Miller, S., and Herrmann, A. M.: Metabolising old soil carbon: Simply a matter of simple organic matter?, *Soil Biol. Biochem.*, 88, 128–136, <https://doi.org/10.1016/j.soilbio.2015.05.018>, 2015.
- 570
- Parikh, S. J., Goynes, K. W., Margenot, A. J., Mukome, F. N. D., and Calderón, F. J.: Soil chemical insights provided through vibrational spectroscopy, 1–148 pp., <https://doi.org/10.1016/B978-0-12-800132-5.00001-8>, 2014.
- Paul, E. A.: The nature and dynamics of soil organic matter: Plant inputs, microbial transformations, and organic matter stabilization, *Soil Biol. Biochem.*, 98, 109–126, <https://doi.org/10.1016/j.soilbio.2016.04.001>, 2016.
- 575
- R Core Team: R: A language and environment for statistical computing, <https://www.r-project.org/>, 2020.
- Reheis, M. C., Bright, J., Lund, S. P., Miller, D. M., Skipp, G., and Fleck, R. J.: A half-million-year record of paleoclimate from the Lake Manix Core, Mojave Desert, California, *Palaeogeogr. Palaeoclimatol. Palaeoecol.*, 365–366, 11–37, <https://doi.org/10.1016/j.palaeo.2012.09.002>, 2012.
- 580
- Ryals, R., Kaiser, M., Torn, M. S., Berhe, A. A., and Silver, W. L.: Impacts of organic matter amendments on carbon and nitrogen dynamics in grassland soils, *Soil Biol. Biochem.*, 68, 52–61, <https://doi.org/10.1016/j.soilbio.2013.09.011>, 2014.
- Schmidt, M. W. I., Torn, M. S., Abiven, S., Dittmar, T., Guggenberger, G., Janssens, I. A., Kleber, M., Kögel-Knabner, I., Lehmann, J., Manning, D. A. C., Nannipieri, P., Rasse, D. P., Weiner, S., and Trumbore, S. E.: Persistence of soil organic matter as an ecosystem property, *Nature*, 478, 49–56, <https://doi.org/10.1038/nature10386>, 2011.
- 585
- Six, J., Paustian, K., Elliott, E. T., and Combrink, C.: Soil Structure and Organic Matter I. Distribution of Aggregate-Size Classes and Aggregate-Associated Carbon, *Soil Sci. Soc. Am. J.*, 64, 681–689, <https://doi.org/10.2136/sssaj2000.642681x>, 2000.
- Sollins, P., Kramer, M. G., Swanston, C., Lajtha, K., Filley, T., Aufdenkampe, A. K., Wagai, R., and Bowden, R. D.: Sequential density fractionation across soils of contrasting mineralogy: Evidence for both microbial- and mineral-controlled soil organic matter stabilization, *Biogeochemistry*, 96, 209–231, <https://doi.org/10.1007/s10533-009-9359-z>, 2009.

- 590 Spielvogel, S., Prietzel, J., and Kögel-Knabner, I.: Soil organic matter stabilization in acidic forest soils is preferential and soil type-specific, *Eur. J. Soil Sci.*, 59, 674–692, <https://doi.org/10.1111/j.1365-2389.2008.01030.x>, 2008.
- Sposito, G., Skipper, N. T., Sutton, R., Park, S. H., Soper, A. K., and Greathouse, J. A.: Surface geochemistry of the clay minerals, *Proc. Natl. Acad. Sci. U. S. A.*, 96, 3358–3364, <https://doi.org/10.1073/pnas.96.7.3358>, 1999.
- Stotzky, G. and Rem, L. T.: Influence of clay minerals on microorganisms. I. Montmorillonite and kaolinite on bacteria., *Can. J. Microbiol.*, 12, 547–563, <https://doi.org/10.1139/m66-078>, 1966.
- Todd-Brown, K. E. O., Randerson, J. T., Post, W. M., Hoffman, F. M., Tarnocai, C., Schuur, E. A. G., and Allison, S. D.: Causes of variation in soil carbon simulations from CMIP5 Earth system models and comparison with observations, 10, 1717–1736, <https://doi.org/10.5194/bg-10-1717-2013>, 2013.
- 600 Viscarra Rossel, R. A., Behrens, T., Ben-Dor, E., Brown, D. J., Demattê, J. A. M., Shepherd, K. D., Shi, Z., Stenberg, B., Stevens, A., Adamchuk, V., Aichi, H., Barthès, B. G., Bartholomeus, H. M., Bayer, A. D., Bernoux, M., Böttcher, K., Brodský, L., Du, C. W., Chappell, A., Fouad, Y., Genot, V., Gomez, C., Grunwald, S., Gubler, A., Guerrero, C., Hedley, C. B., Knadel, M., Morrás, H. J. M., Nocita, M., Ramirez-Lopez, L., Roudier, P., Campos, E. M. R., Sanborn, P., Sellitto, V. M., Sudduth, K. A., Rawlins, B. G., Walter, C., Winowiecki, L. A., Hong, S. Y., and Ji, W.: A global spectral library to characterize the world's soil, *Earth-Science Rev.*, 155, 198–230, <https://doi.org/10.1016/j.earscirev.2016.01.012>, 2016.
- 605 Vranova, V., Rejsek, K., and Formanek, P.: [Aliphatic, Cyclic, and Aromatic Organic Acids, Vitamins, and Carbohydrates in Soil: A Review](#), *Sci. J.*, 2013, [524239](#), 2013.
- [Wei, Y., Wu, X., Xia, J., Shen, X., Cai, C.: Variation of Soil Aggregation along the Weathering Gradient: Comparison of Grain Size Distribution under Different Disruptive Forces](#), *PLoS ONE*, 11: e0160960. doi:10.1371/journal.pone.0160960, 2016.
- 610 White, A. F., Blum, A. E., Schulz, M. S., Bullen, T. D., Harden, J. W., and Peterson, M. L.: Chemical Weathering of a Soil Chronosequence on Granite Alluvium I. Reaction Rates Based on Changes in Soil Mineralogy, *Geochim. Cosmochim. Acta*, 60, 2533–2550, 1996.
- White, A. F., Schulz, M. S., Vivit, D. V., Blum, A. E., Stonestrom, D. A., and Harden, J. W.: Chemical weathering rates of a soil chronosequence on granitic alluvium: III. Hydrochemical evolution and contemporary solute fluxes and rates, *Geochim. Cosmochim. Acta*, 69, 1975–1996, <https://doi.org/10.1016/j.gca.2004.10.003>, 2005.
- 615 Xu, Y., He, J., Cheng, W., Xing, X., and Li, L.: Natural ^{15}N abundance in soils and plants in relation to N cycling in a rangeland in Inner Mongolia, *J. Plant Ecol.*, 3, 201–207, <https://doi.org/10.1093/jpe/rtq023>, 2010.
- Yang, Y., Ji, C., Chen, L., Ding, J., Cheng, X., and Robinson, D.: Edaphic rather than climatic controls over ^{13}C enrichment between soil and vegetation in alpine grasslands on the Tibetan Plateau, *Funct. Ecol.*, 29, 839–848, <https://doi.org/10.1111/1365-2435.12393>, 2015.
- 620 Zhao, Q., Poulson, S. R., Obrist, D., Sumaila, S., Dynes, J. J., McBeth, J. M., and Yang, Y.: Iron-bound organic carbon in forest soils: Quantification and characterization, 13, 4777–4788, <https://doi.org/10.5194/bg-13-4777-2016>, 2016.



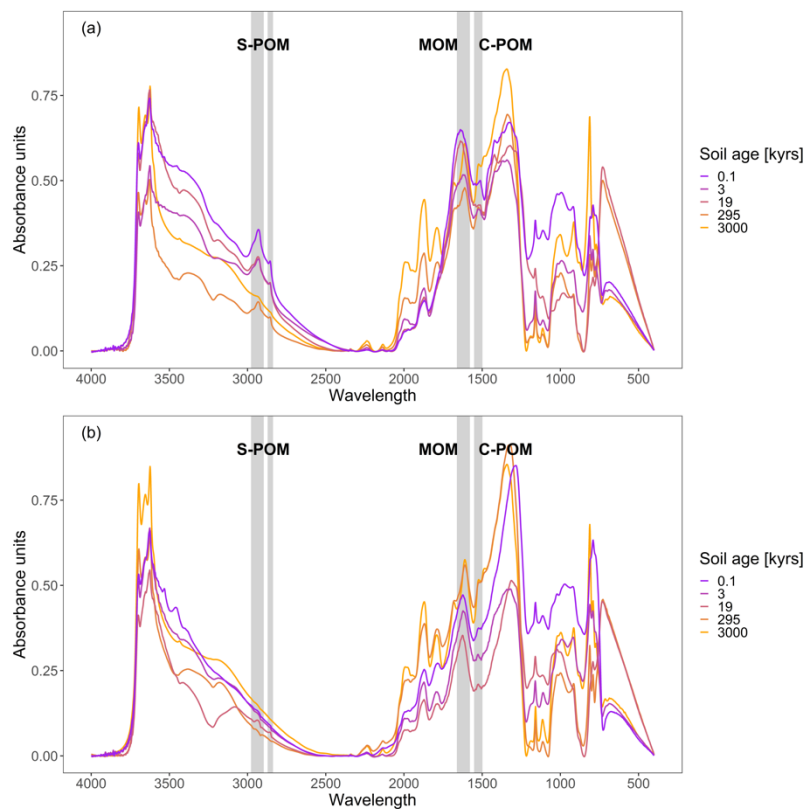


625

Figure 1: Map of the study area based on a digital elevation model (DEM) retrieved from Shuttle Radar Topography Mission (SRTM, resolution ~ 30 m). River hydrology data was taken from Lehner et al. (2008).

Table 1: Overview of wavenumber ranges used to calculate absorbance peak areas from DRIFTS, the respective functional groups related to specific biochemical properties of SOM compounds and compiled information on the origin (Demyan et al., 2012; Parikh et al., 2014; Hall et al., 2018) and the respective SOM properties (C:N ratio, $\delta^{13}\text{C}$, and $\delta^{15}\text{N}$ values) of each functional group (Benner et al., 1987; Austin and Vitousek, 1998; Dijkstra et al., 2006; Xu et al., 2010; Vranova et al., 2013).

SOM type	Wavenumber center (range) [cm^{-1}]	Functional group	Origin	SOM properties
S-POM	2925 (2976-2898) + 2850 (2870-2839)	aliphatic C-H stretch	constituent of litter, component of many root exudates (i.e. citrate, oxalate)	intermediate C:N ratio, $\delta^{13}\text{C}$ and $\delta^{15}\text{N}$ depleted compared to soil but higher compared to C- POM
C-POM	1525 (1550-1500)	aromatic C=C stretch	mostly lignin, related to wooden plant parts, also found in root constituents and aromatic root exudates (i.e. phthalic or vanillic)	high C:N ratio, $\delta^{13}\text{C}$ and $\delta^{15}\text{N}$ depleted
MOM	1620 (1660-1580)	amide, quinone, ketone C=O stretch, aromatic C=C and/or carboxylate C-O stretch	constituents of microbial cell walls (amides and quinones), and long-chained lipids (ketones)	low C:N ratio, $\delta^{13}\text{C}$ and $\delta^{15}\text{N}$ enriched



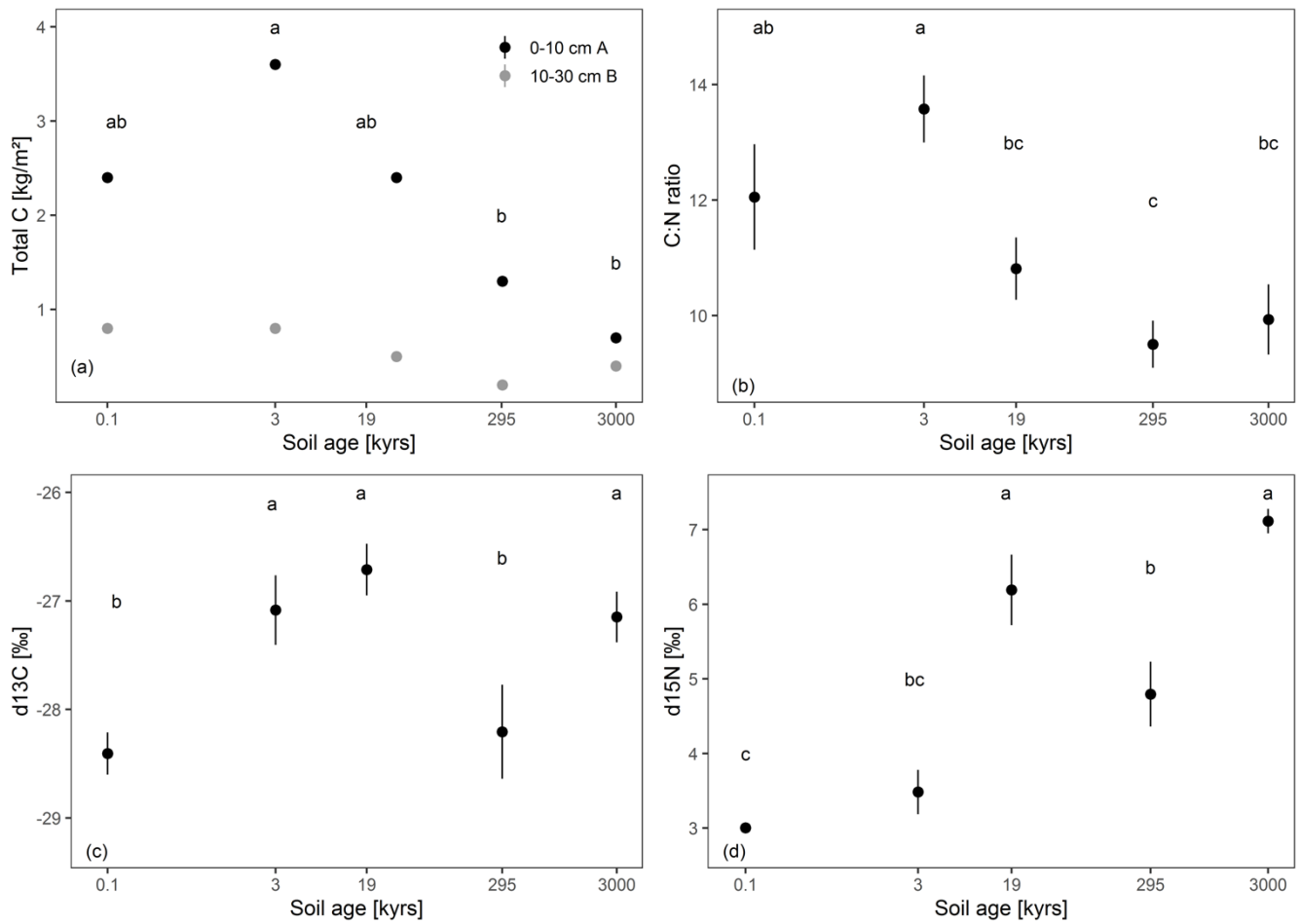
635 **Figure 2: Baseline corrected DRIFTS spectra of each soil age for 0-10 cm (2a) and 10-30 cm (2b) soil depth. The wavenumber ranges across which absorbance peak areas were integrated for functional group assignment are indicated with grey bars in the background. The two wavenumber ranges around 2900 cm^{-1} stand for simple plant-derived OM (S-POM), the one around 1620 cm^{-1} for microbially-associated OM (MOM), and the one at 1525 cm^{-1} for complex plant-derived OM (C-POM).**

Table 2: Overview of soil mineralogy and texture changes with increasing soil age in 0-10 and 10-30 cm depth (n = 30). The mineralogy was measured using inductively coupled plasma-atomic emission spectrometry (ICP-AES). Texture was quantified with a laser diffraction particle size analyser. Pedogenic oxides were extracted in duplicates with dithionite-citrate-bicarbonate (DCB).

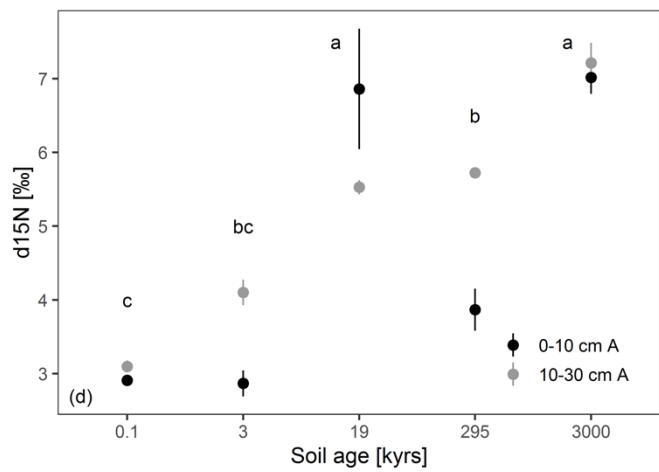
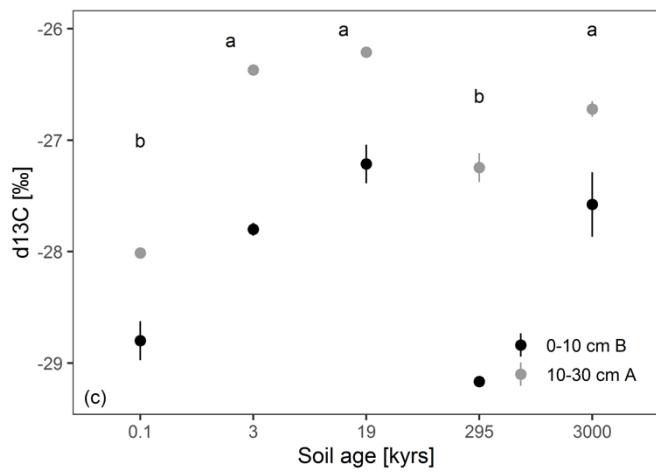
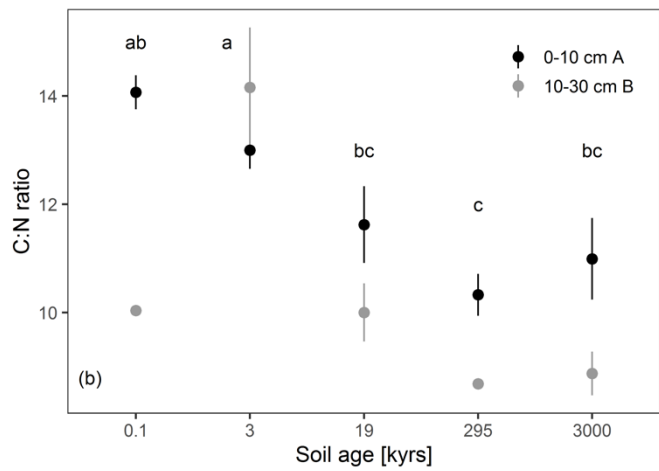
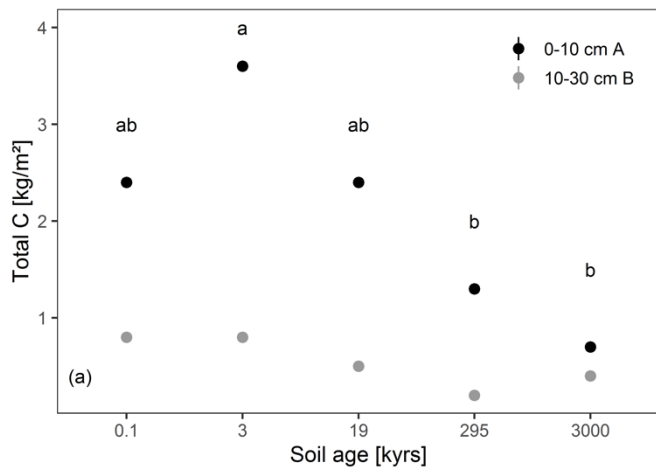
Soil depth [cm]	Soil age [kyr]	Al _{total} [g/kg]	Fe _{total} [g/kg]	Si _{total} [g/kg]	Fe _{total} /Si _{total}	Al _{DCB} [g/kg]	Fe _{DCB} [g/kg]	Fe _{total} /Fe _{DCB}	Al _{total} /Al _{DCB}	Ti:Zr	Clay [%]	Silt [%]	Sand [%]	CEC [meq/100g]	B _{sat} [%]	pH
0-10	0.1	82.7	36.5	241.	0.15	1.3	6.2	5.9	65.1	21.6	15.2	58.4	26.4	15.2	86.6	6.8
0-10	3	65.0	35.3	293.	0.12	1.0	9.5	3.7	66.2	19.6	9.1	62.6	28.2	13.4	109.	6.6
0-10	19	81.1	38.4	267.	0.14	1.1	6.6	7.6	86.9	26.8	11.2	64.3	24.5	24.7	81.1	5.9
0-10	295	63.9	18.2	338.	0.05	0.7	6.2	2.9	88.5	13.8	13.7	50.3	36.0	4.6	103.	6.1
0-10	3000	29.3	23.1	393.	0.06	1.3	13.6	1.7	22.3	10.8	11.1	68.1	20.8	4.5	58.3	4.7
10-	0.1	92.2	37.1	280.	0.13	1.0	6.1	6.1	102.	18.0	4.9	63.1	32.0	14.2	74.3	6.8
10-	3	73.4	39.6	306.	0.13	0.9	10.4	3.8	80.3	14.2	12.9	69.2	17.9	9.9	116.	6.2
10-	19	87.1	43.7	273.	0.16	1.3	7.2	6.4	84.7	24.4	17.4	69.3	13.4	20.8	95.5	6.0
10-	295	64.9	18.4	348.	0.05	0.6	6.5	2.8	106.	14.6	19.0	53.3	27.7	2.1	131.	5.8
10-	3000	36.7	25.3	389.	0.06	1.4	13.5	1.9	26.2	10.1	18.3	69.2	12.5	2.1	85.3	4.3

Table 2: Overview of soil mineralogy and texture changes with increasing soil age in 0-10 and 10-30 cm depth (n = 10). The mineralogy was measured using inductively coupled plasma-atomic emission spectrometry (ICP-AES). Texture was quantified with a laser diffraction particle size analyser. Pedogenic oxides were extracted in duplicates with dithionite-citrate-bicarbonate (DCB).

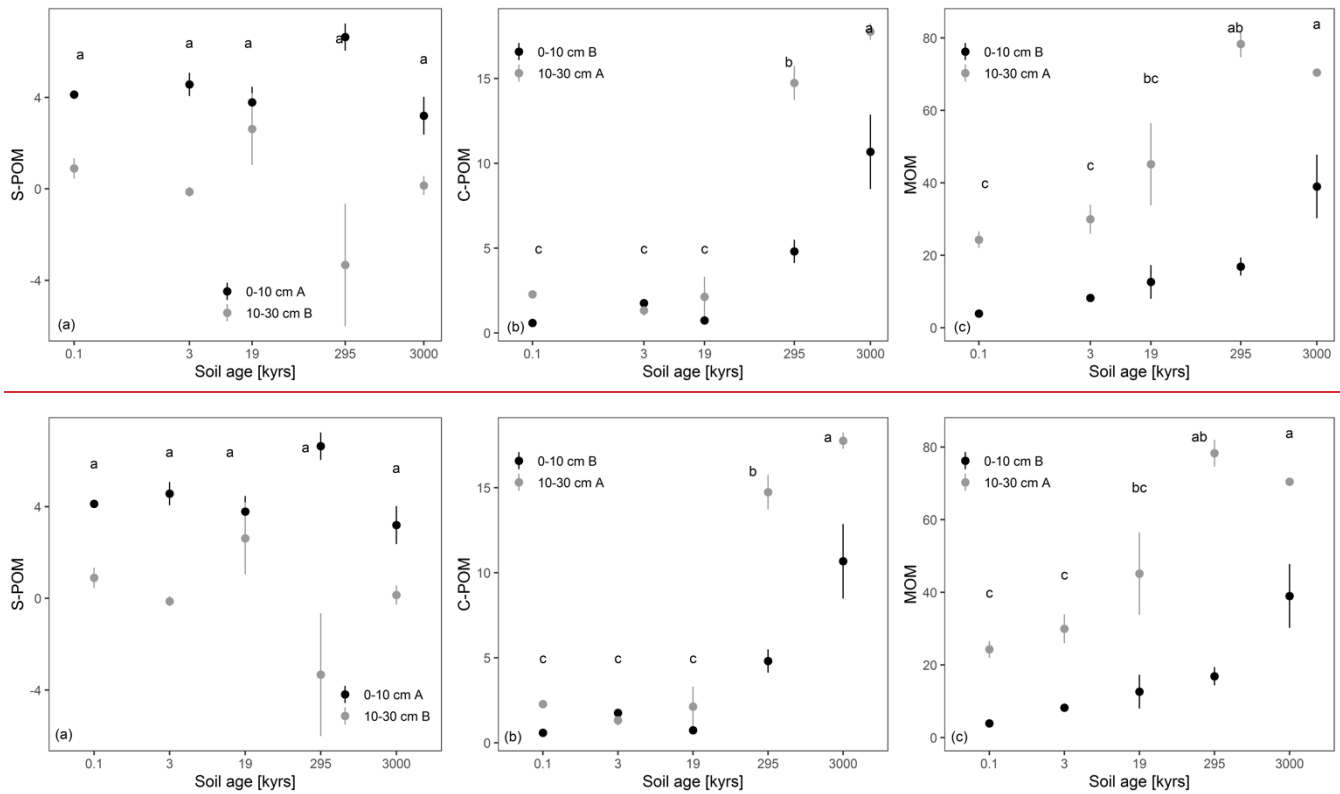
Soil depth [cm]	Soil age [kyrs]	Al _{total} [g/kg]	Fe _{total} [g/kg]	Si _{total} [g/kg]	Fe _{total} /Si _{total}	Al _{DCB} [g/kg]	Fe _{DCB} [g/kg]	Fe _{total} /Fe _{DCB}	Al _{total} /Al _{DCB}	Ti:Zr	Clay [%]	Silt [%]	Sand [%]	CEC [meq/100g]	B _{sat} [%]	pH
0-10	0.1	82.7	36.5	241.5	0.15	1.3	6.2	5.9	65.1	21.68	15.2	58.4	26.4	15.2	86.6	6.8
0-10	3	65.0	35.3	293.1	0.12	1.0	9.5	3.7	66.2	19.62	9.1	62.6	28.2	13.4	109.4	6.6
0-10	19	81.1	38.4	267.2	0.14	1.1	6.6	7.6	86.9	26.85	11.2	64.3	24.5	24.7	81.1	5.9
0-10	295	63.9	18.2	338.6	0.05	0.7	6.2	2.9	88.5	13.82	13.7	50.3	36.0	4.6	103.7	6.1
0-10	3000	29.3	23.1	393.4	0.06	1.3	13.6	1.7	22.3	10.86	11.1	68.1	20.8	4.5	58.3	4.7
10-30	0.1	92.2	37.1	280.3	0.13	1.0	6.1	6.1	102.8	18.07	4.9	63.1	32.0	14.2	74.3	6.8
10-30	3	73.4	39.6	306.2	0.13	0.9	10.4	3.8	80.3	14.22	12.9	69.2	17.9	9.9	116.6	6.2
10-30	19	87.1	43.7	273.0	0.16	1.3	7.2	6.4	84.7	24.42	17.4	69.3	13.4	20.8	95.5	6.0
10-30	295	64.9	18.4	348.0	0.05	0.6	6.5	2.8	106.8	14.60	19.0	53.3	27.7	2.1	131.2	5.8
10-30	3000	36.7	25.3	389.4	0.06	1.4	13.5	1.9	26.2	10.13	18.3	69.2	12.5	2.1	85.3	4.3



645 **Figure 3: Mean \pm standard deviation of site triplicates of total C (3a), the C:N ratio (3b), $\delta^{13}\text{C}$ (3c), and $\delta^{15}\text{N}$ (3d) for 0-10 cm (black) and 10-30 cm soil depth (grey). Significant differences between the soil ages calculated with the Tukey-HSD test are indicated with letters ($p < 0.05$). Differences across soil age are indicated with lowercase letters, differences across soil depth in capital letters. Soil age is spaced based on the log-transformed age differences.**



650



655

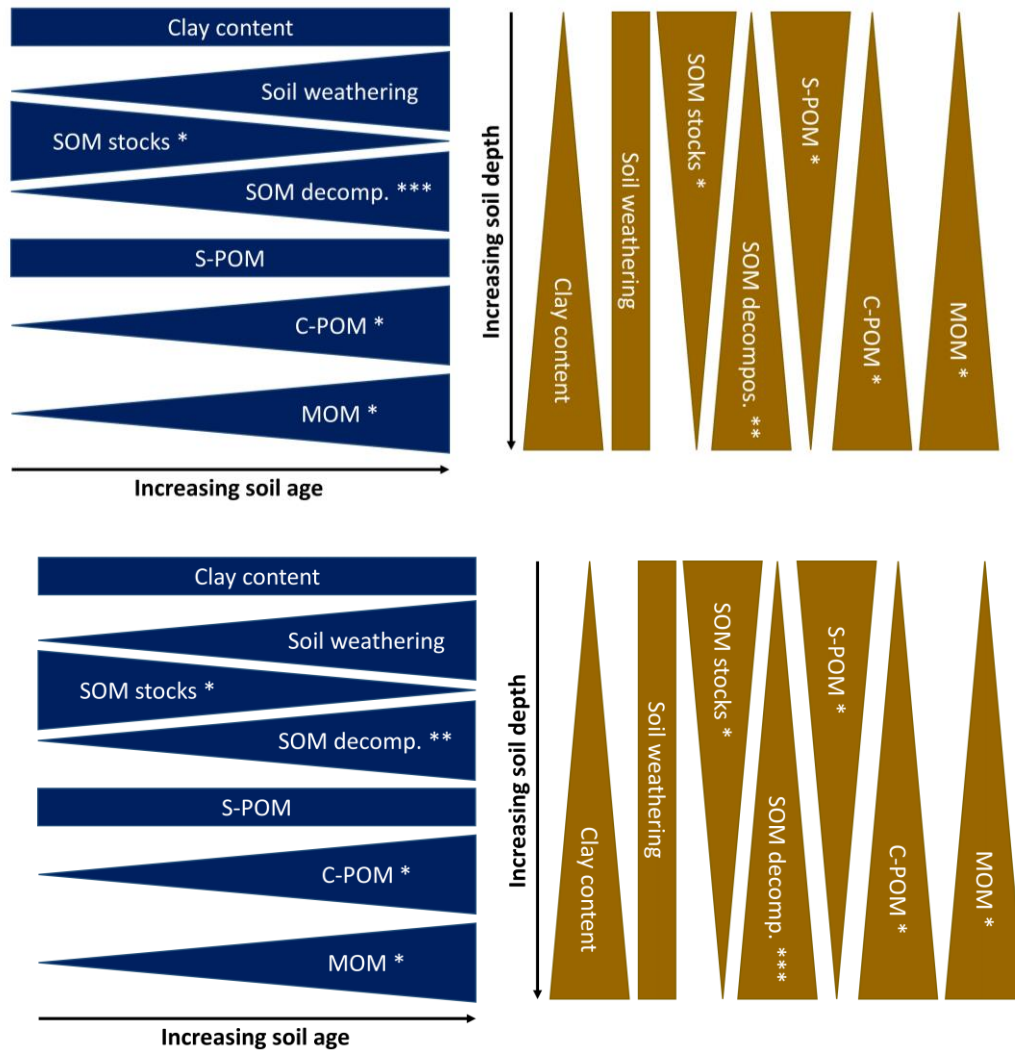
Figure 4: Mean \pm standard deviation of site triplicates of the DRIFTS absorbance peak areas (unitless) corresponding to simple plant-derived OM (S-POM; 4a), complex plant-derived OM (C-POM; 4b), and mainly microbial-derived OM (MOM; 4c) for 0-10 cm (black) and 10-30 cm soil depth (grey). Homogeneous subgroups ($p < 0.05$) across soil age are indicated with letters. Significant differences between soil depth are indicated with letters behind the depth classes in the legend. The subgroups were identified by pairwise comparison (Tukey-HSD) following a two-way ANOVA ($n = 30$). Soil age is spaced based on the log-transformed age differences.

660

665

Table 3: Overview of the linear regression models describing SOM composition (C:N ratio, $\delta^{15}\text{N}$ and $\delta^{13}\text{C}$), and peak areas of functional groups related to simple plant-derived OM (S-POM), complex plant-derived OM (C-POM) and mainly microbially-derived OM (MOM) based on $n = 30$ observations. Explanatory variables related to the mineral matrix and soil texture were selected (Al_{DCB} , Fe_{DCB} , $\text{Fe}_{\text{total}}:\text{Si}_{\text{total}}$ ratio, clay content). **Absolute and relative model fit parameters (root mean squared error (RMSE and rRMSE), mean absolute error (MAE and rMAE), and R^2) with standard deviations were computed following 100 iterations of a Monte-Carlo cross-validation. Higher coefficients of variable importance indicate a higher importance of the variable to explain the impact on the regression slope. The significance levels of each model parameter on the linear model are denoted as $p < 0.001$ (***) and $p < 0.01$ (**), respective response variable.**

	C:N ratio	$\delta^{15}\text{N}$	$\delta^{13}\text{C}$	S-POM	C-POM	MOM
RMSE	2.0 ± 0.5	1.2 ± 0.5	0.6 ± 0.2	2.9 ± 1.0	3.2 ± 0.7	20.3 ± 5.7
R^2	0.32 ± 0.27	0.64 ± 0.24	0.61 ± 0.32	0.39 ± 0.33	0.78 ± 0.10	0.57 ± 0.27
Coefficients of variable importance						
Al_{DCB}	1.3	1.3	3.3	2.3	1.0	1.1
Fe_{DCB}	1.8	0.6	5.2	2.1	1.0	1.6
$\text{Fe}_{\text{total}}:\text{Si}_{\text{total}}$	3.2	1.4	5.0	1.4	5.0	0.8
Clay	0.4	1.5	4.1	2.2	2.8	3.7
	<u>C:N ratio</u>	<u>$\delta^{15}\text{N}$</u>	<u>$\delta^{13}\text{C}$</u>	<u>S-POM</u>	<u>C-POM</u>	<u>MOM</u>
<u>RMSE</u>	<u>2.0 ± 0.5</u>	<u>1.2 ± 0.5</u>	<u>0.6 ± 0.2</u>	<u>2.9 ± 1.0</u>	<u>3.2 ± 0.7</u>	<u>20.3 ± 5.7</u>
<u>rRMSE</u>	<u>17.9</u>	<u>24.4</u>	<u>-2.2</u>	<u>128.9</u>	<u>56.3</u>	<u>61.7</u>
<u>MAE</u>	<u>1.8 ± 0.4</u>	<u>1.0 ± 0.4</u>	<u>0.6 ± 0.1</u>	<u>2.5 ± 0.9</u>	<u>2.6 ± 0.7</u>	<u>18.1 ± 5.5</u>
<u>rMAE</u>	<u>16.1</u>	<u>20.3</u>	<u>-2.2</u>	<u>111.1</u>	<u>45.8</u>	<u>55.1</u>
<u>R^2</u>	<u>0.32 ± 0.27</u>	<u>0.64 ± 0.24</u>	<u>0.61 ± 0.32</u>	<u>0.39 ± 0.33</u>	<u>0.78 ± 0.10</u>	<u>0.57 ± 0.27</u>
<u>Coefficients of variable importance</u>						
<u>Al_{DCB}</u>	<u>1.3</u>	<u>1.3</u>	<u>3.3 **</u>	<u>2.3</u>	<u>1.0</u>	<u>1.1</u>
<u>Fe_{DCB}</u>	<u>1.8</u>	<u>0.6</u>	<u>5.2 ***</u>	<u>2.1</u>	<u>1.0</u>	<u>1.6</u>
<u>$\text{Fe}_{\text{total}}:\text{Si}_{\text{total}}$</u>	<u>3.2 **</u>	<u>1.4</u>	<u>5.0 ***</u>	<u>1.4</u>	<u>5.0</u>	<u>0.8</u>
<u>Clay</u>	<u>0.4</u>	<u>1.5</u>	<u>4.1 ***</u>	<u>2.2 **</u>	<u>2.8 **</u>	<u>3.7 **</u>



670 Figure 5: Conceptual model explaining the influence of soil development with increasing soil age and depth on mineralogy and texture based on our findings. These properties (i.e. $F_{e_{total}:Si_{total}}$, $F_{e_{CB}}$) may then drive the dynamics of SOM stocks, properties, and composition. SOM stocks reflect the total C stock, SOM decomposition proxies include $\delta^{13}C$, $\delta^{15}N$, and the C:N ratio, and the signals of the selected DRIFTS peak areas are represented individually. ~~Duplicates of s~~Soil weathering proxies and clay content were not tested since only one value per soil age and depth was available (n = 10). SOM decomposition proxies and peak areas were tested by a two-way ANOVA (n = 30) with Tukey-HSD as post-hoc test (p < 0.05): * showed significant trends. ** significant trends for C:N and $\delta^{15}N$ but not for $\delta^{13}C$. *** significant trends for C:N and $\delta^{13}C$ but not for $\delta^{15}N$. The outcomes of the ANOVA are visualized in Fig. 3 and 4, the values of soil geochemistry in Table 2.

675